

Identification of a Novel BCL2 Specific Inhibitor that Binds Predominantly to the BH1 Domain

Divyaanka Iyer^{1*}, Supriya V. Vartak^{1*}, Archita Mishra^{2#}, Gunaseelan Goldsmith^{3#}, Sujeet Kumar^{4#},
Mrinal Srivastava^{1#}, Mahesh Hegde¹, Vidya Gopalakrishnan^{1,3}, Mark Glenn⁵, Mahesh Velusamy³,
Bibha Choudhary³, Nagesh Kalakonda⁵, Subhas S. Karki⁴, Avadhesh Surolia²
and Sathees C. Raghavan^{1**}

From ¹Department of Biochemistry, Indian Institute of Science, Bangalore 560 012, India, ²Molecular Biophysics Unit, Indian Institute of Science, Bangalore 560 012, India, ³Institute of Bioinformatics and Applied Biotechnology, Electronics City, Bangalore 560 100, India, ⁴Department of Pharmaceutical Chemistry, KLE University's College of Pharmacy, Bangalore 560 010, India, ⁵Haematology, Department of Molecular and Clinical Cancer Medicine University of Liverpool, Liverpool L69 3GA, U K

Running title: Identification of a novel inhibitor of BCL2

Article type : Original Article

*Equal first authors; #Equal second authors

**To whom correspondence should be addressed: Department of Biochemistry, Indian Institute of Science, Bangalore-560012, Ph. +91 80 22932674; Fax: +91 80 23600814;

e-mail: sathees@biochem.iisc.ernet.in

Key words: Small molecule inhibitor, Apoptosis, Cancer therapeutics, Genomic instability, Cell death, Chemotherapy, Leukemia, Molecular docking

Abbreviations: Mitochondrial membrane potential (MMP); BCL2 homology (BH); Chronic lymphocytic leukemia (CLL); Circular Dichroism (CD); B-cell lymphoma 2 (BCL2)

This article has been accepted for publication and undergone full peer review but has not been through the copyediting, typesetting, pagination and proofreading process, which may lead to differences between this version and the Version of Record. Please cite this article as doi: 10.1111/febs.13815

This article is protected by copyright. All rights reserved.

ABSTRACT

The antiapoptotic protein BCL2 is overexpressed in several cancers and contributes to prolonged cell survival and chemoresistance, lending itself as an excellent target for cancer therapy. Here we report the design, synthesis and characterization of Disarib, a novel BCL2 inhibitor. Disarib showed selective cytotoxicity in BCL2 high cancer cell lines, and CLL patient primary cells, as compared to BCL2 low cell lines. BCL2 knockdown in cells rendered remarkable resistance to Disarib, while sensitivity was regained upon its ectopic expression, establishing target specificity. *In silico*, biochemical and biophysical studies demonstrated strong affinity of Disarib to BCL2, but not to other antiapoptotic BCL2 family members viz., BCL-xL, BCL2A1 etc. Interestingly, biophysical studies showed that BH1 domain deletion mutant demonstrated ~67-fold reduction in BCL2-Disarib interaction, while it was only ~20-fold in case of BH3 deletion mutant, suggesting predominant involvement of the BH1 domain for Disarib binding. Thus, we report identification of a novel BCL2 inhibitor with a unique mechanism of BCL2 inhibition, as opposed to the well-studied BH3 domain targeting.

INTRODUCTION

Apoptosis, a physiological process of programmed cell death, is crucial during both development and regulation of normal cell proliferation in differentiated tissues [1]. It involves a complex network of protein-protein interactions that relies on the balance between antiapoptotic (BCL2, BCL-xL, BCL2A1, BCLw and MCL1) and proapoptotic (BAX, BAK, BAD, BID, PUMA and BIM) proteins [2, 3]. Antiapoptotic proteins possess four BCL2 homology domains (BH1, BH2, BH3 and BH4) and a C-terminal transmembrane domain. Proapoptotic proteins have BH1, BH2, BH3 and transmembrane domains [4]. The proapoptotic proteins upon homodimerization form pores in the mitochondrial membrane, leading to mitochondrial outer membrane permeabilization releasing apoptotic factors [4].

Hyperproliferation and survival in many malignancies is attributed to the upregulation of antiapoptotic proteins, BCL2 and BCL-xL. BCL2 upregulation has been reported in B-cell lymphomas and leukemias (60-80%), colorectal adenocarcinomas (90%), breast cancer (70%) and prostate cancer (30-60%), and additionally in lung and nasopharyngeal carcinomas [5-7]. Besides, BCL2 overexpression is a feature of many chemoresistant tumors [8, 9]. Hence, treatment modalities that either target BCL2 alone or in combination with other drugs, are desirable. Since the physiological level of BCL2 in normal dividing cells is low, it is considered an attractive cancer therapeutic target. Moreover, BCL2 overexpressing cells become sensitive to cell death upon its inhibition, even in the presence of other antiapoptotic proteins [10].

Three classes of previously reported BCL2 inhibitors include BCL2 antisense oligonucleotides [11], BH3 derived peptides [12, 13] and BH3-targeted small molecule inhibitors [14]. Among these, small molecule inhibitors are gaining prominence due to their amenability to design, development and *in vivo* administration. Prominent examples of this class include YC137 [15], ABT737 [16], ABT199 [17] and Tw37 [18]. Among these, YC137 and ABT199 are BCL2 specific, while ABT737 and Tw37 are pan active [19].

Many BCL2 inhibitors target its well conserved BH3 domain [17, 20]. Apparently, specificity for ABT199 is conferred by a hydrogen bond involving Asp103 in the BH3 domain of BCL2 (Asp 103 is replaced by Glu 103 in BCL-xL). Therefore, binding of an inhibitor to differential residues in the hydrophobic groove can be an effective strategy for BCL2 specificity. Although all the antiapoptotic BCL2 family members engage the proapoptotic partners along their hydrophobic groove, sequence variability and subtle conformational differences among them can be exploited to design specific inhibitors.

In the current study, we report the design, synthesis and characterization of a novel small molecule inhibitor, Disarib. Disarib confers selective sensitivity to BCL2 overexpressing cells and acts in a target specific manner both in leukemic cell lines and primary cancer cells derived from patients. Disarib binds predominantly to BH1 domain of BCL2 and does not interfere significantly with other members of the BCL2 anti-apoptotic family.

RESULTS

Design of potential novel BCL2 inhibitors- 3-substituted indolin-2-one compounds are known to possess anticancer properties [21, 22]. A molecule of this class, Z24 with antiangiogenic properties was considered as a potential BCL2 inhibitor due to its ability to dock onto BCL2 *in silico* and exhibit moderate cytotoxicity against cells with ectopic BCL2 expression [23]. In the present study, we have used chemical backbones derived from Z24 to evaluate their relative affinities to BCL2 *in silico*, with the objective of obtaining more specific and effective BCL2 inhibitors. A chemical backbone **5** was found to dock into the BCL2 hydrophobic cleft that acts as a receptacle for the BH1 and BH3 domains of proapoptotic proteins (Fig. 1A, B). Thus, a panel of 17 derivatives of backbone **5** possessing varying alkyl substitutions was generated (**5a-5t**), and chemically and biologically characterized (Fig. 1C-E). Docking studies revealed their binding onto the BCL2 hydrophobic groove with different binding affinities (data not shown). Among the panel of molecules, the compound **5m**, renamed Disarib, showed the most favourable binding energy (-10.4 kcal/mol).

Screening of potential BCL2 inhibitors for target specificity- Synthesized compounds were tested for target specificity in cells with varying levels of endogenous BCL2 expression. Leukemia cell lines, NALM6 and CEM (high BCL2 expression) and chronic myelogenous leukemia cell line, K562 (low BCL2 expression), were chosen for further studies [24]. Results showed that **5a, 5b, 5c, 5e, 5f, 5g, 5m** and **5o** exhibited low IC₅₀ values (2-4 μ M) (Table 2). Further analysis for BCL2 specificity showed

that **5m** (Disarib) and **5t** were the only molecules that displayed activity in a target dependent manner. Interestingly, Disarib exhibited the lowest IC₅₀ values in both CEM and NALM6, while its effect on K562 was ~6 times lower as compared to NALM6 (Table 2). Hence, Disarib was further characterized by NMR, and LC-MS (Fig. 2A-B). The structure of Disarib is composed of a central imidazothiadiazole ring A, flanked by benzyl and phenyl rings (B, C) and an indole ring (D) placed in parallel and antiparallel directions (Fig. 2C).

Disarib induces cytotoxicity in various cancer cell lines in a BCL2 level dependent manner- The cytotoxic effects of Disarib were compared in various cancer cell lines and a noncancerous cell line (293T). Results showed that viability was significantly reduced at 48 h of treatment in cells expressing higher levels of BCL2 (REH, NALM6, CEM P388D1, A2780, Molt4), while cells with low BCL2 (K562, T47D, 293T, HeLa, LNCaP) exhibited reduced cytotoxicity (Fig. 3A,B). Interestingly, the effect was minimal in the noncancerous cell line, 293T (Fig. 3A,B). Thus our data suggests that Disarib-induced cytotoxicity is correlated with the levels of BCL2 expression.

To rule out the possibility that cytotoxic effect of Disarib is dependent on the electrophilic properties of the chemical backbone used for generating the series of potential BCL2 inhibitors, we compared the cytotoxicity induced by Disarib with that of inactive compound **5p** as a control. Live-dead cell assay results showed a distinct difference between the sensitivity of NALM6 cells when exposed to Disarib, as compared to **5p** (data not shown).

Knockdown and ectopic expression of BCL2 affects Disarib sensitivity in cells- In order to determine the correlation between observed Disarib sensitivity in cells and BCL2 expression, siRNA mediated knockdown of BCL2 in NALM6 cells was performed. siRNA concentration of 250 nM was chosen as it reduced BCL2 expression by ~80% in NALM6 cells (Fig. 4A). NALM6 cells were transfected with either *BCL2*-specific or scrambled siRNA 24 h prior to the addition of Disarib. Results showed a dose-dependent decrease in the sensitivity of cells to Disarib upon BCL2 knockdown (Fig. 4B) suggesting a direct correlation between level of BCL2 expression and Disarib sensitivity. Importantly, we also find that Disarib treatment (5 μM) following restoration of BCL2 levels (pCMV-SPORT-BCL2, ~80% expression as compared to controls) imparts significant cytotoxicity, in contrast to BCL2 knockdown cells (Fig. 4C,D). Importantly, it is possible that Disarib, upon binding to BCL2 protein, disrupts the interaction between BCL2 and its proapoptotic partners such as BAK or BAX, subsequently leading to apoptosis. Thus, the loss of BCL2 function, due to Disarib administration could lead to the observed cytotoxicity. In contrast, siRNA mediated knockdown of BCL2 will result in decrease in expression of the BCL2 protein and that might allow other antiapoptotic proteins to take over potential BCL2 function inside cells, preventing cytotoxicity. Consistent to this, there are reports of cells compensating the downregulation of their main antiapoptotic protein by the upregulation of another antiapoptotic protein that is functionally redundant [25]. A similar mechanism may be operational during down regulation of BCL2 expression and may explain the observed cell viability.

In order to further confirm the target specificity of Disarib, other members of BCL2 family proteins, MCL1 and BCL2A1 were overexpressed in NALM6 cells (Fig. 4E), and subsequently subjected to Disarib treatment (5 μ M). Interestingly, overexpression of MCL1 and BCL2A1 did not affect the sensitivity of cells to Disarib, confirming its BCL2-specific action (Fig. 4F).

Taken together, these results demonstrate BCL2 dependency of Disarib activity, thereby confirming its specificity.

Disarib binds to BCL2, but not to other antiapoptotic BCL2 family proteins- In order to test whether Disarib can bind to BCL2 directly, by occupying the hydrophobic proapoptotic BH3 binding groove, detailed *in silico* docking studies were performed. Using AutoDock Vina [26], Disarib was docked with full length BCL2 as well as with transmembrane truncated BCL2 (Fig. 5A). The Disarib binding pocket of BCL2 is defined by residues D103, F104, Y108, V133, N143, W144, F153 and V199 (encompassing the region between helices α 2, loop b/w α 2 & α 3, α 5 and α 7) along the hydrophobic groove of BCL2 (Fig. 1B). The aromatic ring A (imidazo[2,1-b][1,3,4]thiadiazole) of Disarib is placed at the centre of the binding pocket and stacks well with the aromatic ring of F104. One of the nitrogen atoms of ring A is involved in hydrogen bond interaction with main chain amino group (-NH-) of the well conserved G145 of BH1 domain, while the other nitrogen atom engages in hydrogen bond interaction with the side chain OH group of Y108. The sulphur atom of ring A is involved in hydrogen bond interaction with N δ 2 group of N143 (with N ϵ and N δ 2 group of R146 and N143, respectively in truncated BCL2). The Br atom of ring C engages in hydrogen bond interaction with OH group of Y202. Ring C is also involved in van der Waals interaction with highly conserved W144 (ring C is involved in π - π stacking interaction with indole ring of W144 in truncated BCL2). R146 of the well conserved NWGR motif is involved in cation- π interaction with ring B, while Cl atom of ring B engages in hydrogen bond interaction with side chain amino group of R139 (cation- π interaction involving side chain amino group of R146 and ring B in truncated BCL2). Nitrogen and oxygen moieties of ring D makes hydrogen bond interaction with invariant D103 and R107 of BH3 domain (Fig. 5A).

Further, we compared interaction of Disarib with BCL2, with that of other members of the antiapoptotic family, such as BCL-xL, BCL2A1, MCL1 and BCLw. To examine the interaction of Disarib with BCL-xL, it was docked with crystal structure of BCL-xL (PDB ID: 1R2D) (Fig. 5B) and studied for binding. In comparison to BCL2, Disarib binds with less affinity along the hydrophobic groove of BCL-xL owing to conformational difference between these two proteins. It is seen that the hydrophobic groove of BCL-xL exhibits lesser volume ($\sim 260 \text{ \AA}^3$) than BCL2 ($\sim 350 \text{ \AA}^3$) due to difference in length and orientation of helix 3 between the two proteins (data not shown). This results in a slightly narrow groove in BCL-xL vis-à-vis BCL2 (Fig 6A; black ellipse; denoted by cyan and blue arrows for BCL2 and BCL-xL). Apparently this disallows Disarib to be placed comfortably in the binding pocket of BCL-xL due to steric clashes arising between ring D and ring C of Disarib with

residues R100 and Y195 in BCL-xL. This is not seen in case of BCL2 due to differential spatial positioning of Arginine residue compared to BCL-xL (R107 vs R100) (Fig. 5B; 6A). As a consequence, hydrogen bond interaction involving R139 (of highly conserved NWGR motif), E96, Y101 and π - π interaction involving F97 and Disarib are not feasible in case of BCL-xL as opposed to their counterpart in BCL2 (R146, D103, Y108 and F104) (Fig. 5A,B). These features could account for the less binding affinity of Disarib towards BCL-xL vis-à-vis BCL2. This observation is corroborated by less binding energy of Disarib in binding to BCL-xL (-5.7 kcal/mol) as compared to its interaction with BCL2 (-10.4 kcal/mol).

To examine the binding specificity of Disarib with BCL2A1, it was docked with crystal structure of BCL2A1 (PDB ID:2VM6) and studied for interaction (Fig. 5C). In comparison to BCL2, Disarib binds with less affinity along the hydrophobic groove of BCL2A1, owing largely to the difference in amino acid composition along the hydrophobic binding pocket (overall the two proteins share only ~25% sequence identity) and a conformational difference in the orientation of helix containing BH3 domain in the two proteins. This results in less stabilising interactions in BCL2A1. Crucial interactions involving F104, Y108 with ring A, R139 with ring B and R107 with ring D seen in BCL2 are not feasible in BCL2A1. This seemingly renders Disarib to bind with less affinity to BCL2A1. This is corroborated by less binding energy (-4.5 kcal/mol) for BCL2A1 vis-à-vis BCL2 (-10.4 kcal/mol).

In addition, we also tested the binding specificity of Disarib with MCL1, by docking it with the NMR structure of MCL1 (PDB ID: 2MHS) and studied for interaction (Fig. 5D). In comparison to BCL2, Disarib seemingly binds with less affinity along the hydrophobic groove of MCL1, owing largely to the difference in amino acid composition along the binding pocket located between BH1 and BH3 domains in the two proteins. Interestingly, the two proteins share only ~24% sequence identity. Residues from the conserved NWGR motif viz., side chain of N260 and main chain amino group (-NH-) of G262 are engaged in hydrogen bond interaction with the sulphur and one of the nitrogen atoms of ring A. Ring C is involved in π - π interaction with F319, while chlorine substituent of ring B forms a weak CH...O interaction with side chain of V258. Likewise, nitrogen atom of 2-Oxindole ring (ring D) forms hydrogen bond with side chain of N223. However, crucial interactions involving F104, Y108 with ring A, R139 with ring B and R107 with ring D seen in BCL2 are not seen in MCL1. These features account for the less binding affinity of Disarib with MCL1 and is further reflected by less binding energy (-5.1 kcal/mol) as opposed to BCL2 (-10.4 kcal/mol).

To determine the binding specificity of Disarib with BCLw, it was docked with NMR structure of BCLw (PDB ID: 1ZY3) and studied for interaction (Fig. 5E). In comparison to BCL2, Disarib binds with less affinity along the hydrophobic groove of BCLw, owing to considerable conformational difference (RMSD = ~3.1 Å for 122 C^α atoms) between these two enzymes. This leads to differential placement of the conserved residues and results in less stabilising interactions between BCLw and Disarib (data not shown). Vital interactions involving G145, F104, Y108 with ring A,

R139 with ring B and D103 as well as R107 with ring D seen in BCL2 are not feasible in BCLw. This seemingly renders Disarib to bind with less affinity to BCLw (-6.0 kcal/mol).

To test whether Disarib can interact with BCL2 or its paralogues, recombinant BCL2, BCL-xL and BCL2A1 proteins were overexpressed and purified (Fig. 6B-D). In order to confirm the high affinity of Disarib to BCL2, thermal shift assays [27-30] were performed using purified BCL2 and its homologue proteins BCL-xL and BCL2A1. Thermal stability of BCL2 protein was enhanced with increase in Disarib concentration, which is indicated as an increase in T_m upon ligand addition (Fig. 6E). However, addition of purified BCL-xL or BCL2A1 showed no significant shift in T_m even at 100 μ M Disarib (Fig. 6F,G; data not shown). This demonstrates that Disarib binding is exclusive to BCL2 protein and its observed proapoptotic effect is BCL2 specific. The dissociation constant (K_d) of Disarib for BCL2 was calculated to be 28 nM (Fig. 6E). CD spectroscopic studies showed that Disarib (10, 50, 75, 100 and 150 nM) can bind to purified BCL2 in a dose-dependent manner resulting in conformational changes of BCL2 (Fig. 6H). Comparison of Disarib binding pattern with BCL2 and BCL-xL showed a clear shift in the spectrum of BCL2, but not in the case of BCL-xL, indicating direct and specific binding of BCL2 and Disarib (Fig. 6H, I). When truncated BCL2 protein (terminal 69 amino acids truncation including transmembrane and a part of BH2 domain) was used, Disarib binding to BCL2 was also observed in a concentration dependent manner (data not shown). Further, CD studies showed that similar to BCL-xL, Disarib failed to bind to the proapoptotic protein, BAK (data not shown).

Disarib predominantly binds to the BH1 domain of BCL2- The BCL2 family proteins have well conserved domains, viz. BH1, BH2, BH3, BH4 and the transmembrane domain. Docking studies with full length BCL2 suggested that Disarib interacts with both BH1 and BH3 domains of BCL2, however, the interaction with BH1 domain was predominant, with several highly conserved residues contributing in anchoring the inhibitor. This could explain observed greater affinity of BCL2 with Disarib compared to other antiapoptotic proteins such as MCL1. Since BH1 domain in BCL2 seems crucial in binding, it would be interesting to see if other anti-apoptotic family members like MCL1 would also exhibit more sensitivity towards Disarib, if the BH1 domain was swapped with that from BCL2. To test this, a homologue model of MCL1 with BH1 domain swapped with that of BCL2 was built using Modeller 9v7 and docking studies were carried out.

It is to be noted that the BH1 domain (loop intervening helices α_4 & α_5 , followed by helix α_5) of BCL2 (20 AA) and MCL1 (21 AA) share a sequence identity of ~57% and differ in their structures by ~ 2 Å RMSD (19 C α atoms), with deviation seen largely in the loop region (data shown). Docking studies had indicated that 4 highly conserved and 1 semi-conserved residues from the BH1 domain of BCL2 interact with Disarib, while only 2 highly and 1 partially-conserved residues of wild type MCL1 was observed to interact with Disarib (Fig. 5A,D; Table 3). When the BH1 domain of MCL1 is swapped with that of BCL2, two additional strong interactions with Disarib emerge, involving R263 (well conserved; α_5) and R255 (partially-conserved; loop b/w α_4 and α_5),

besides interactions involving N260 and G262 seen with the wild type (Fig. 7A, B [left panels]; Table 3). R255 engages in a strong hydrogen bond interaction with Cl atom of ring B, while R263 is involved in cation... π interaction with ring B of Disarib (Fig. 7B, left panel). Other interactions involving residues of BH3 domain and $\alpha 7$ are retained (Fig. 7A,B left panels). Thus, these additional interactions originating from the BH1 domain (of swapped BCL2) seem to increase the sensitivity of MCL1 towards Disarib, as reflected in the enhanced binding energy of -7.7 kcal/mol vis-à-vis -5.1 kcal/mol seen earlier with the wild type MCL1. It is thus obvious that BCL2 confers preferential binding for Disarib compared to other antiapoptotic proteins with crucial interactions emerging from its BH1 domain (Table 3).

Further to establish the domain responsible for BCL2-Disarib interaction, we resorted to biophysical approaches using BCL2 domain deleted mutants. Using site directed mutagenesis, two independent BCL2 mutant constructs, BH1 domain deleted (Δ BH1) and BH3 deleted (Δ BH3), were generated. Proteins were over expressed in bacteria, purified (Fig. 7C, D) and studied using thermal shift assays (Fig. 7E-G). Interestingly, we observed that compared to wild type purified BCL2 protein, which showed a binding constant of 28 nM upon Disarib interaction (Fig. 7E), the Δ BH1 protein showed a Kd of 1.8 μ M, which was ~67 fold higher than the wild type BCL2 protein (Fig. 7F). On the other hand, the binding constant for Δ BH3 protein was 537 nM, which was 20 fold higher than the wild type BCL2 protein (Fig. 7G). These results suggested a weak binding of Δ BH3 protein compared to the wild type BCL2, but a less severe loss in binding efficiency as compared to the BH1 domain deletion. Overall, our observations establish that BH1 domain of BCL2 predominantly interacts with Disarib, followed by BH3, to a lesser extent. Further, this result gives an experimental correlation to *in silico* docking studies where we have demonstrated that BH1 domain provides crucial interface for Disarib binding to a significantly greater extent than BH3 domain. More importantly these findings shed light on a novel mode of BCL2 inhibition, by predominantly targeting the BH1 domain, as opposed to other BCL2 inhibitors which target mostly BH3 domain of BCL2.

Disarib induces significant cytotoxicity in CLL patient primary cells and mouse tumor models-

Further, we investigated the potential of Disarib as an anti-cancer molecule in patient-derived cells 'high' for BCL2 levels. Robust expression of BCL2 has been reported in chronic lymphocytic leukemia (CLL) patients [31, 32]. Primary cells from six patients were tested for their sensitivity to Disarib. Results showed initiation of apoptosis in 40% of cells after 4 h of treatment in a dose-dependent manner (Fig. 8A, B). However, the percentage of cells undergoing cell death varied among patients. Thus, our data suggests that Disarib can induce apoptosis in primary patient cells.

In order to investigate the efficacy of Disarib in an *in vivo* model system, a BCL2- driven mouse tumor model (Dalton's Lymphoma) was chosen for the study [33]. Disarib (10 mg/kg b.wt.; 6 doses) was administered via an intraperitoneal route in mice following induction of DLA tumor. Interestingly, Disarib treatment resulted in significant reduction in tumor progression, as compared to that in the untreated control (Fig. 9A). Further, a comparative analysis was performed using

previously characterized BCL2 inhibitors (HA 14-1, Gossypol, Epigallocatechin), along with Disarib in the DLA mouse tumor model (Fig. 9B). An identical dosage regime was followed in case of each inhibitor (10 mg/kg, 6 doses on alternate days). Interestingly, among the inhibitors tested, Disarib exhibited highest potential leading maximal tumor regression, followed by Gossypol [19, 20]. While HA 14-1 was effective to a limited extent, Epigallocatechin did not result in any significant tumor reduction. Taken together, these results highlight the potential of Disarib in hampering tumor cell growth in a mouse model and its effectiveness, as compared to other known BCL2 inhibitors (Fig. 9B).

Body weight fluctuation is one of the important parameters commonly employed for assessing the adverse effects of a drug on normal physiology. In order to investigate effect of Disarib on the overall health of normal animals, mice were treated with Disarib and monitored for change in body weight over a period of 16 days (Fig. 9C). Interestingly, results showed no significant change in body weight in Disarib treated mice, as compared to that of untreated control group, indicating nontoxic nature of Disarib in normal mice (Fig. 9C).

Disarib activates the apoptotic cascade in cancer cells- We further investigated the mechanism of cell death induced by Disarib using various assays. Disarib treated cells were subjected to Annexin FITC/PI double-staining in order to assess the cell death pathway activated. Results showed predominant activation of the apoptotic pathway (Fig. 10A), after 48 h of Disarib treatment, with no significant increase in the necrotic cell population (Fig. 10A,B). Interestingly, Disarib treated cells stained with Hoechst dye showed significant increase in cells with nuclear condensation, a hallmark of apoptosis (Fig. 10C). Further, Dalton's lymphoma cells from mouse tumor ascites were treated with increasing concentrations of Disarib (0, 10, 20 μ M), followed by assessment of characteristic markers for intrinsic and extrinsic apoptotic pathway. Interestingly, activated Caspase 9 showed increased expression in Disarib treated cells in a concentration dependent manner as compared to untreated tumor controls, indicating activation of the intrinsic apoptotic pathway (Fig. 10D). Cleavage of PARP in Disarib treated cells reiterated activation of apoptosis (Fig. 10D). Interestingly, Caspase 8 cleavage was undetectable in treated samples (Fig. 10D). Taken together, Disarib activated apoptosis via the intrinsic pathway, and caused cell death in mouse tumor cells.

Thus, our results identify a novel inhibitor of BCL2, which acts in a target specific manner, and does not cross-react with other members of the anti-apoptotic family (Fig. 11). Disarib predominantly targets the BH1 domain of BCL2, thus exhibiting a novel mode of BCL2 inhibition. Results show that it effectively causes cytotoxicity in cancer cell lines with high BCL2 expression, and in CLL patient cells.

DISCUSSION

In the present study, we have identified a novel small molecule inhibitor of BCL2, Disarib, which effectively acts in a target specific manner against various BCL2 high cancer cells. Its cytotoxic property correlates with BCL2 expression as evidenced by knockdown and overexpression studies, further supporting its specificity. Our studies with CLL patient samples confirm the ability of Disarib to initiate apoptosis in primary cancer cells. Further, *in vitro* studies show a binding selectivity of Disarib to BCL2 over BCL-xL and BCL2A1.

One of the reasons of Disarib specificity for BCL2 and not to other antiapoptotic BCL2 family members viz., BCL-xL, BCL2A1 might be due to subtle conformational difference (BCL2 vs BCL-xL) and amino acid composition variability (BCL2 vs BCL2A1) along the hydrophobic groove of these proteins. Particularly, the design of Disarib with branching oxindole ring D leads to steric clashes in BCL-xL, whereas it is comfortably placed in BCL2 partly due to spatial difference in presence of a bulky arginine residue (R107 in BCL2 and R100 in BCL-xL) in these two proteins. Besides, it was noted that flexibility of Disarib to interact with W137, R139 (well conserved NWGR motif), E96, F97 and Y101 are restricted due to steric contacts with R100 and Y195 in BCL-xL, whereas their counterparts (R107, Y108, D103, N143, G145, R146) in BCL2 stabilizes the interaction with Disarib. Interestingly, ring D is engaged in electrostatic interaction with the invariant arginine (R107) and aspartic acid (D103) in BCL2, whereas this interaction is not feasible in BCL-xL thereby contributing to the specificity (Fig. 5A,B). Small size (less molecular weight) of Disarib compared to ABT199 adds to its advantage.

A major highlight of the present study is the ability of Disarib to interact predominantly with BH1 domain of the BCL2 hydrophobic pocket. *In silico* docking analyses predict several key residues of the BH1 domain to be important for Disarib anchoring to BCL2. However, results also suggest residues E96, F97 and Y101 of the BH3 domain to be involved during Disarib-BCL2 interaction. Interestingly, our biophysical studies using BH1 and BH3 domain deleted BCL2 mutants show a ~20 fold decrease in Disarib binding in case of BH3 domain deletion, while the effect was more severe (~67 fold reduction) upon BH1 domain deletion. The decreased binding of BH1 domain mutants argue for a predominant involvement of the BH1 domain for Disarib binding, followed by BH3 domain, to a lesser extent. The observed mode of Disarib binding presents a novel mechanism of BCL2 inhibition, as opposed to the well-studied BH3 domain only targeting strategies.

Among various BCL2 inhibitors studied, one of the most impressive examples is the Nur77 peptide [34] which was described to cause conformational changes in BCL2, converting it to a proapoptotic protein. While this mode of inhibition provides conceptual insight for future drug design, it is yet to be developed as a therapeutic tool. This is true even in the case of antisense therapy against BCL2, which has found better use in combinatorial modalities, but has limitations as a single agent [10]. Although several small molecule inhibitors such as ABT737, YC137, Gossypol and HA14-1[14] are described, several of them are pan active [19] with toxic side effects *in vivo*. Gossypol is reported

to be toxic to liver, though its side effects were reduced in its derivative, apogossypol. However, apogossypol is not strictly BCL2 dependent in action [35]. ABT737 by itself, causes limited tumor regression in mouse models and has to be coadministered with other drugs [36], while HA14-1 was shown to be chemically unstable [37]. Unlike other inhibitors, ABT199 is very promising and highly efficient against AML and estrogen dependent breast cancers with enhanced target specificity [38-40]. However, a recent study has indicated that normal mature B cells show acute sensitivity to ABT199 both *in vitro* and *in vivo* [41]. Interestingly, we find that Disarib is specific to BCL2, predominantly targeting the BH1 domain, while sparing other members of the anti-apoptotic family. A notable finding from the current study is the significant tumor regression property of Disarib in a BCL2-driven tumor model. Importantly, when compared with previously characterized BCL2 inhibitors, such as Gossypol, HA 14-1 and Epigallocatechin, Disarib showed higher efficacy, reiterating its potential to be used as a potential chemotherapeutic agent.

Thus, Disarib can be developed as a potent anticancer molecule in a target specific treatment modality, having reduced or no off-target effects.

MATERIALS AND METHODS

Chemistry

2-Amino-5-alkyl/aralkyl-1,3,4-thiadiazoles (**1a-1c**) were prepared from alkyl/ aralkyl acetic acid and thiosemicarbazide as described [42]. The 2-(4-substituted benzyl)-6-(4-substitutedaryl)-imidazo[2,1-*b*][1,3,4]thiadiazole derivatives (**3a-3t**) were prepared by reaction of 2-amino-5-alkyl/aralkyl-1,3,4-thiadiazoles (**1a-1c**) with the appropriate phenacyl bromide (**2**), and neutralization with cold aqueous sodium carbonate to get the free base with 50-60% yield (Fig. 1A-C; Table 1). The various phenacyl bromides were prepared by bromination of the corresponding ketones in glacial acetic acid. Appropriate aldehydes (**4a-4t**) were obtained in turn by means of the Vilsmeier Haack reaction on the corresponding imidazo[2,1-*b*][1,3,4]thiadiazoles (**3a-3t**). The 2-[(2-(4-substitutedbenzyl)-6-phenylimidazo[2,1-*b*][1,3,4]thiadiazol-5-yl)methylidene]-1,2-dihydro-3H-indol-3-one (**5a-5t**) were prepared by reaction between aldehydes (**4a-4t**) and 2-indolinone in methanol, in the presence of catalytic amount of piperidine with good yields (Fig. 1C, Table 1)

5-benzyl-1,3,4-thiadiazol-2-amine (**1a**), 5-(4-chlorobenzyl)-1,3,4-thiadiazole (**1b**), 2-benzyl-6-(4'-fluorophenyl)imidazo[2,1-*b*][1,3,4]-thiadiazole (**3i**), 2-(4''-chlorobenzyl)-6-(4'-fluorophenyl)imidazo[2,1-*b*][1,3,4]-thiadiazole (**3n**), 2-benzyl-6-(4'-fluorophenyl)-imidazo[2,1-*b*][1,3,4]-thiadiazole-5-carbaldehyde (**4i**) and 2-(4''-chlorobenzyl)-6-(4'-fluorophenyl)imidazo[2,1-*b*][1,3,4]-thiadiazole-5-carbaldehyde (**4n**) were prepared according to literature [42]. 6-(4'-chlorophenyl)-2-methylimidazo[2,1-*b*][1,3,4]-thiadiazole (**3p**), 6-(4'-bromophenyl)-2-methylimidazo[2,1-*b*][1,3,4]-thiadiazole (**3q**), 6-(4'-chlorophenyl)-2-methylimidazo[2,1-*b*][1,3,4]-thiadiazole-5-carbaldehyde (**4p**), 6-(4'-bromophenyl)-2-methylimidazo[2,1-*b*][1,3,4]-thiadiazole-5-carbaldehyde (**4q**) and 6-(4'-nitrophenyl)-2-methylimidazo[2,1-*b*][1,3,4]-thiadiazole-carbaldehyde

(4r) were prepared according to literature [43]. 2-methyl-6-(4'-nitrophenyl)imidazo[2,1-b][1,3,4]-thiadiazole (3r), 2-methyl-6-(4'-methylphenyl)imidazo[2,1-b][1,3,4]-thiadiazole (3s) and 6-(4'-methoxyphenyl)-2-methyl imidazo[2,1-b][1,3,4]-thiadiazole (3t) were prepared according to literature [44].

General procedure for the preparation of 2-(4''-substitutedbenzyl)-6-(4' substituted phenylimidazo[2,1-b][1,3,4]thiadiazole (3a-3t)- The appropriate 2-amino-5-alkyl/aralkyl-1,3,4-thiadiazole (1) (30 mmol) was treated with the appropriate phenacyl bromide (2) (30 mmol), in ethanol (150 mL). The mixture was refluxed for 10-12 h. Excess of solvent was removed under reduced pressure and the solid hydrobromide was separated by filtration, washed with cold ethanol and dried. Neutralization of hydrobromide salts with cold aqueous solution of sodium carbonate yielded the corresponding free base which was filtered with a yield of 52-62%.

2-benzyl-6-(4-bromophenyl)imidazo[2,1-b][1,3,4]-thiadiazole (3a)- Yield 52%. IR ν_{\max} (cm⁻¹) 3148, 3028, 2910, 1516, 1479, 1397, 1284, 1005. ¹H-NMR (CDCl₃, 400 MHz) δ (ppm): 4.30 (2H, s, -CH₂-), 7.31-7.40 (5H, m, ar), 7.52 (2H, d, $J = 8$), 7.68 (2H, d, $J = 8$), 7.96 (1H, s, im). +ESI (m/z): 371.9 (M+2).

2-benzyl-6-(4-chlorophenyl)imidazo[2,1-b][1,3,4]-thiadiazole (3b)- Yield 58% IR ν_{\max} cm⁻¹ 3128, 3062, 3031, 2916, 1524, 1470, 1402, 1092. +ESI (m/z): 326.1 [M+1].

2-benzyl-6-(4-methoxyphenyl)imidazo[2,1-b][1,3,4]-thiadiazole (3c)- Yield 55%. IR ν_{\max} cm⁻¹ 3133, 3062, 3029, 2960, 1611, 1548, 1489, 1303, 1245, 1095. ¹H-NMR (CDCl₃, 400 MHz) δ (ppm): 3.84 (3H, s, OCH₃), 4.32 (2H, s, -CH₂-), 6.97 (2H, d, $J = 8$), 7.31-7.41 (5H, m, ar), 7.74 (2H, d, $J = 8$), 7.88 (1H, s, im). +ESI (m/z): 322.0 (M+1).

2-benzyl-6-(4-methylphenyl)imidazo[2,1-b][1,3,4]-thiadiazole (3d)- Yield 54%. IR ν_{\max} cm⁻¹ 3118, 3073, 2973, 1604, 1477, 1259, 1197, 1059. ¹H-NMR (DMSO-d₆, 400 MHz) δ (ppm): 2.30 (3H, s, CH₃), 4.43 (2H, s, -CH₂-), 7.20 (2H, d, $J = 8$), 7.29-7.41 (5H, m, ar), 7.73 (2H, d, $J = 8$), 8.55 (1H, s, im). +ESI (m/z): 306.0 (M+1).

2-(4-chlorobenzyl)-6-phenylimidazo[2,1-b][1,3,4]-thiadiazole (3e)- Yield 53%. IR ν_{\max} cm⁻¹ 3100, 3068, 2910, 1604, 1528, 1483, 1435, 1193, 1020. ¹H-NMR (CDCl₃, 400 MHz) δ (ppm): 4.27 (2H, s, -CH₂-), 7.25-7.31 (3H, m, ar), 7.34-7.42 (4H, m, ar), 7.80 (2H, d, $J = 8$), 7.97 (1H, s, im).

2-(4-chlorobenzyl)-6-(4-chlorophenyl)imidazo[2,1-b][1,3,4]-thiadiazole (3f)- Yield 58%. IR ν_{\max} cm⁻¹ 3147, 3057, 2945, 2860, 1531, 1485, 1410, 1089. ¹H-NMR (CDCl₃, 400 MHz) δ (ppm): 4.27 (2H, s, -CH₂-), 7.27 (2H, d, $J = 8$), 7.35-7.38 (4H, dd, $J = 8, 8$), 7.94 (1H, s, im). +ESI (m/z): 360.0 (M).

2-(4-chlorobenzyl)-6-(4-methylphenyl)imidazo[2,1-b][1,3,4]-thiadiazole (3g)- Yield 54%. IR ν_{\max} cm⁻¹ 3143, 3055, 2927, 2861, 1528, 1476, 1403, 1092. ¹H-NMR (CDCl₃, 400 MHz) δ (ppm): 2.37 (3H, s, -CH₃), 4.26 (2H, s, -CH₂-), 7.22 (2H, d, $J = 8$), 7.27 (2H, d, $J = 8$), 7.36 (2H, d, $J = 8$), 7.69 (2H, d, $J = 8$), 7.92 (1H, s, im). +ESI (m/z): 340.0 (M).

2-(4-chlorobenzyl)-6-(4-methoxyphenyl)imidazo[2,1-b][1,3,4]-thiadiazole (3h)- Yield 52%. IR ν_{\max} cm^{-1} 3146, 3040, 2939, 2842, 1609, 1537, 1482, 1252, 1025. $^1\text{H-NMR}$ (CDCl_3 , 400 MHz) δ (ppm): 3.84 (3H, s, OCH_3), 4.26 (2H, s, $-\text{CH}_2-$), 6.96 (2H, d, $J = 8$), 7.27 (2H, d, $J = 8$), 7.36 (2H, d, $J = 8$), 7.73 (2H, d, $J = 8$), 7.88 (1H, s, im). +ESI (m/z): 356.0 (M).

2-benzyl-6-(4-fluorophenyl)imidazo[2,1-b][1,3,4]-thiadiazole (3i)- Yield 51%. IR ν_{\max} cm^{-1} 3136, 3065, 2923, 1598, 1545, 1524, 1470, 1222, 1156, 1055. +ESI (m/z): 310.1 [M+1].

2-benzyl-6-phenylimidazo[2,1-b][1,3,4]-thiadiazole (3j)- Yield 50%. IR ν_{\max} cm^{-1} 3130, 3061, 2920, 1601, 1540, 1520, 1472, 1225, 1151, 1049. $^1\text{H-NMR}$ (CDCl_3 , 400 MHz) δ (ppm): 4.30 (2H, s, $-\text{CH}_2-$), 7.27-7.42 (8H, m, ar), 7.78-7.81 (2H, m, ar), 7.96 (1H, s, im). +ESI (m/z): 292.2 (M+1).

2-benzyl-6-(4-nitrophenyl)imidazo[2,1-b][1,3,4]-thiadiazole (3k)- Yield 60%. IR ν_{\max} cm^{-1} 3129, 2925, 2827, 1598, 1508, 1337, 1189, 1101, 1062. $^1\text{H-NMR}$ (DMSO-d_6 , 400 MHz) δ (ppm): 4.46 (2H, s, $-\text{CH}_2-$), 7.29-7.42 (5H, m, ar), 8.10 (2H, d, $J = 8$), 8.27 (2H, d, $J = 8$), 8.92 (1H, s, im). +ESI (m/z): 337.0 (M+1).

2-(4-chlorobenzyl)-6-(4-nitrophenyl)imidazo[2,1-b][1,3,4]-thiadiazole (3l)- Yield 53%. IR ν_{\max} cm^{-1} 3130, 2925, 1598, 1503, 1414, 1185, 1098, 1017. $^1\text{H-NMR}$ (DMSO-d_6 , 400 MHz) δ (ppm): 4.47 (2H, s, $-\text{CH}_2-$), 7.44 (4H, s, ar), 8.09 (2H, d, $J = 8$), 8.26 (2H, d, $J = 8$), 8.91 (1H, s, im). -ESI (m/z): 369.0 (M-1).

2-(4-chlorobenzyl)-6-(4-bromophenyl)imidazo[2,1-b][1,3,4]-thiadiazole (3m)- Yield 55%. IR ν_{\max} cm^{-1} 3149, 3055, 2927, 1590, 1528, 1082, 1007. $^1\text{H-NMR}$ (CDCl_3 , 400 MHz) δ (ppm): 4.27 (2H, s, $-\text{CH}_2-$), 7.27 (2H, d, $J = 8$), 7.37 (2H, d, $J = 8$), 7.53 (2H, d, $J = 8$), 7.68 (2H, d, $J = 8$), 7.96 (1H, s, im). +ESI (m/z): 405.9 (M+1).

2-(4-chlorobenzyl)-6-(4-fluorophenyl)imidazo[2,1-b][1,3,4]-thiadiazole (3n)- Yield 56%. IR ν_{\max} cm^{-1} 3140, 3116, 3042, 2918, 1537, 1482, 1412, 1227, 1148, 1092. $^1\text{H-NMR}$ (DMSO-d_6 , 400 MHz) δ (ppm): 4.45 (2H, s, $-\text{CH}_2-$), 7.20-7.24 (2H, m, ar), 7.48 (4H, s, ar), 7.84-7.88 (2H, m, ar), 8.61 (1H, s, im). +ESI (m/z): 344.0 (M).

3-(2-(4-chlorobenzyl)imidazo[2,1-b][1,3,4]thiadiazol-6-yl)-2H-chromen-2-one-(3o)- Yield 51%. IR ν_{\max} cm^{-1} 3145, 3045, 2973, 1729, 1609, 1484, 1102. $^1\text{H-NMR}$ (DMSO-d_6 , 400 MHz) δ (ppm): 4.48 (2H, s, $-\text{CH}_2-$), 7.40 (1H, t, $J = 16$), 7.45 (5H, m, ar), 7.61 (1H, t, $J = 16$), 7.87 (1H, d, $J = 8$), 8.56 (1H, s, ar), 8.66 (1H, s, im). -ESI (m/z): 392.0 (M-1).

General procedure for the preparation of [2-(4-substituted benzyl)-6-(4'-substituted phenylimidazo[2,1-b][1,3,4]thiadiazole-5-carbaldehyde) (4a-4t)-The Vilsmeier Haack reagent was prepared at 0-5°C by dropping POCl_3 (2.3 g, 15 mmol) into a stirred solution of DMF (10 ml). The appropriate imidazo[2,1-b][1,3,4]thiadiazole **3** (4 mmol) was added slowly to the Vilsmeier reagent while stirring and cooling was maintained for 2 h. Further stirring was continued for 6 h at 80-90°C. The resulting reaction mixture was poured into 100 ml of water; the precipitate was filtered, pressed,

suspended in water and neutralized to pH 7 with cold aqueous solution of sodium carbonate. The solid was separated by filtration, washed with water, dried and crystallized from EtOH with a yield of 40-55 %.

2-benzyl-6-(4-bromophenyl)imidazo[2,1-b][1,3,4]-thiadiazole-5-carbaldehyde (4a)- Yield 55%. IR ν_{\max} cm^{-1} 3069, 3025, 2908, 2850, 1683, 1476, 1300, 1119. $^1\text{H-NMR}$ (CDCl_3 , 400 MHz) δ (ppm): 4.45 (2H, s, $-\text{CH}_2-$), 7.31-7.44 (5H, m, ar), 7.65 (2H, d, $J = 8$), 7.76 (2H, d, $J = 8$), 10.07 (1H, s, -CHO). +ESI (m/z): 400 [M+2].

2-benzyl-6-(4-chlorophenyl)imidazo[2,1-b][1,3,4]-thiadiazole-5-carbaldehyde (4b)- Yield 51%. IR ν_{\max} cm^{-1} 3077, 3028, 2930, 1672, 1626, 1483, 1191, 1092. $^1\text{H-NMR}$ (CDCl_3 , 400 MHz) δ (ppm): 4.45 (2H, s, $-\text{CH}_2-$), 7.34-7.41 (5H, m, ar), 7.49 (2H, d, $J = 8$), 7.82 (2H, d, $J = 8$), 10.06 (1H, s, -CHO). +ESI (m/z): 356.1 [M+2].

2-benzyl-6-(4-methoxyphenyl)imidazo[2,1-b][1,3,4]-thiadiazole-5-carbaldehyde (4c)- Yield 49%. IR ν_{\max} cm^{-1} 3052, 2998, 2837, 1650, 1491, 1180, 1100. ESI (m/z): 350.1 [M+1].

2-benzyl-6-(4-methylphenyl)imidazo[2,1-b][1,3,4]-thiadiazole-5-carbaldehyde (4d)- Yield 51%. IR ν_{\max} cm^{-1} 3100, 3049, 2926, 2861, 1672, 1480, 1186, 1090. $^1\text{H-NMR}$ (CDCl_3 , 400 MHz) δ (ppm): 2.43 (3H, s, $-\text{CH}_3$), 4.45 (2H, s, $-\text{CH}_2-$), 7.32 (2H, d, $J = 8$), 7.34-7.41 (4H, m, ar), 7.72 (2H, d, $J = 8$), 10.02 (1H, s, -CHO). +ESI (m/z): 334.2 [M+1].

2-(4-chlorobenzyl)-6-(4-bromophenyl)imidazo[2,1-b][1,3,4]-thiadiazole-5-carbaldehyde (4e)- Yield 43%. IR ν_{\max} cm^{-1} 3089, 3031, 2978, 2855, 1670, 1601, 1525, 1492, 1191. $^1\text{H-NMR}$ (DMSO-d_6 , 400 MHz) δ (ppm): 4.56 (2H, s, $-\text{CH}_2-$), 7.48 (4H, s, ar), 7.49-7.53 (3H, m, ar), 7.92 (2H, d, $J = 8$), 9.96 (1H, s, -CHO). -ESI (m/z): 352.0 [M-2].

2-(4-chlorobenzyl)-6-(4-chlorophenyl)imidazo[2,1-b][1,3,4]-thiadiazole-5-carbaldehyde (4f)- Yield 46%. IR ν_{\max} cm^{-1} 3318, 3095, 3043, 2929, 2859, 1672, 1484, 1186, 1094. $^1\text{H-NMR}$ (CDCl_3 , 400 MHz) δ (ppm): 4.42 (2H, s, $-\text{CH}_2-$), 7.30 (2H, d, $J = 8$), 7.39 (2H, d, $J = 8$), 7.49 (2H, d, $J = 8$), 7.84 (2H, d, $J = 8$), 10.06 (1H, s, -CHO). -ESI (m/z): 386.0 [M-2].

2-(4-chlorobenzyl)-6-(4-methylphenyl)imidazo[2,1-b][1,3,4]-thiadiazole-5-carbaldehyde (4g)- Yield 48%. IR ν_{\max} cm^{-1} 3033, 2922, 2852, 1664, 1486, 1390, 1184, 1096. $^1\text{H-NMR}$ (DMSO-d_6 , 400 MHz) δ (ppm): 2.36 (3H, s, $-\text{CH}_3$), 4.55 (2H, s, $-\text{CH}_2-$), 7.32 (2H, d, $J = 8$), 7.46 (4H, s, ar), 7.82 (2H, d, $J = 8$), 9.94 (1H, s, -CHO). -ESI (m/z): 366.0 [M-2].

2-(4-chlorobenzyl)-6-(4-methoxyphenyl)imidazo[2,1-b][1,3,4]-thiadiazole-5-carbaldehyde (4h)- Yield 44%. IR ν_{\max} cm^{-1} 3053, 2943, 2839, 1650, 1490, 1388, 1181, 1100. $^1\text{H-NMR}$ (DMSO-d_6 , 400 MHz) δ (ppm): 3.82 (3H, s, $-\text{OCH}_3$), 4.55 (2H, s, $-\text{CH}_2-$), 7.07 (2H, d, $J = 8$), 7.45 (4H, s, ar), 7.92 (2H, d, $J = 8$), 9.95 (1H, s, -CHO).

2-benzyl-6-(4-fluorophenyl)imidazo[2,1-b][1,3,4]-thiadiazole-5-carbaldehyde (4i)- Yield 46%. IR ν_{\max} cm^{-1} 3101, 3025, 2977, 2825, 1675, 1601, 1515, 1482, 1192. $^1\text{H-NMR}$ (DMSO-d_6 , 400 MHz) δ (ppm): 4.56 (2H, s, $-\text{CH}_2-$), 7.32-7.45 (7H, m, ar), 8.01-8.05 (2H, m, ar), 9.98 (1H, s, $-\text{CHO}$). -ESI (m/z): 336.0 [M-1].

2-benzyl-6-phenylimidazo[2,1-b][1,3,4]-thiadiazole-5-carbaldehyde (4j)- Yield 50%. IR ν_{\max} cm^{-1} 3083, 3029, 2975, 2852, 1671, 1600, 1519, 1481, 1187. $^1\text{H-NMR}$ (CDCl_3 , 400 MHz) δ (ppm): 4.46 (2H, s, $-\text{CH}_2-$), 7.34-7.42 (5H, m, ar), 7.48-7.53 (3H, m, ar), 7.81-7.83 (2H, m, ar), 10.04 (1H, s, $-\text{CHO}$). +ESI (m/z): 320.2 [M+1].

2-benzyl-6-(4-nitrophenyl)imidazo[2,1-b][1,3,4]-thiadiazole-5-carbaldehyde (4k)- Yield 45%. IR ν_{\max} cm^{-1} 3085, 2925, 2851, 1675, 1585, 1483, 1398, 1092. $^1\text{H-NMR}$ (DMSO-d_6 , 400 MHz) δ (ppm): 4.45 (2H, s, $-\text{CH}_2-$), 7.35-7.44 (5H, m, ar), 8.19 (2H, d, $J = 9$), 8.33 (2H, d, $J = 9$), 10.20 (1H, s, $-\text{CHO}$). +ESI (m/z): 365.2 [M+1].

2-(4-chlorobenzyl)-6-(4-nitrophenyl)imidazo[2,1-b][1,3,4]-thiadiazole-5-carbaldehyde (4l)- Yield 44%. IR ν_{\max} cm^{-1} 3092, 2935, 1670, 1599, 1520, 1343, 1102. $^1\text{H-NMR}$ (DMSO-d_6 , 400 MHz) δ (ppm): 4.57 (2H, s, $-\text{CH}_2-$), 7.45 (4H, s, ar), 8.26 (2H, d, $J = 8$), 8.32 (2H, d, $J = 8$), 10.06 (1H, s, $-\text{CHO}$). -ESI (m/z): 397.0 [M-2].

2-(4-chlorobenzyl)-6-(4-bromophenyl)imidazo[2,1-b][1,3,4]-thiadiazole-5-carbaldehyde (4m)- Yield 48%. IR ν_{\max} cm^{-1} 3100, 2995, 1675, 1601, 1525, 1345, 1105. $^1\text{H-NMR}$ (DMSO-d_6 , 400 MHz) δ (ppm): 4.55 (2H, s, $-\text{CH}_2-$), 7.44 (4H, s, ar), 7.69 (2H, d, $J = 8$), 7.91 (2H, d, $J = 8$), 9.97 (1H, s, $-\text{CHO}$). -ESI (m/z): 431.9 [M-1].

2-(4-chlorobenzyl)-6-(4-fluorophenyl)imidazo[2,1-b][1,3,4]-thiadiazole-5-carbaldehyde (4n)- Yield 45%. IR ν_{\max} cm^{-1} 3053, 2915, 2840, 1653, 1604, 1492, 1388, 1090. $^1\text{H-NMR}$ (DMSO-d_6 , 400 MHz) δ (ppm): 4.56 (2H, s, $-\text{CH}_2-$), 7.32-7.36 (2H, m, ar), 7.45 (4H, s, ar), 7.99-8.03 (2H, m, ar), 9.96 (1H, s, $-\text{CHO}$). -ESI (m/z): 370.0 [M-2].

2-(4-chlorobenzyl)-6-(2-oxo-2H-chromen-3-yl)imidazo[2,1-b][1,3,4]-thiadiazole-5-carbaldehyde (4o)- Yield 47%. IR ν_{\max} cm^{-1} 3050, 2914, 2856, 1722, 1668, 1483, 1368, 1052. $^1\text{H-NMR}$ (DMSO-d_6 , 400 MHz) δ (ppm): 4.57 (2H, s, $-\text{CH}_2-$), 7.41 (1H, t, $J = 16$), 7.46 (4H, s, ar), 7.50 (1H, d, $J = 8$), 7.69 (1H, t, $J = 16$), 7.88 (1H, d, $J = 8$), 8.51 (1H, s, ar), 9.99 (1H, s, $-\text{CHO}$). -ESI (m/z): 419.9 [M-1].

2-methyl-6-(4'-methylphenyl)imidazo[2,1-b][1,3,4]-thiadiazole-5-carbaldehyde (4s)- Yield 52%. IR ν_{\max} cm^{-1} 3079, 2952, 2859, 1718, 1675, 1480, 1369, 1051.

2-methyl-6-(4'-methoxyphenyl)imidazo[2,1-b][1,3,4]-thiadiazole-5-carbaldehyde (4t)- Yield 55%. IR ν_{\max} cm^{-1} 3098, 2945, 2871, 1712, 1681, 1478, 1375, 1075.

General procedure for the preparation of 3-((2-(4-substitutedbenzyl-6-(4-substitutedphenyl)imidazo[2,1-b][1,3,4]thiadiazol-5-yl) methylidene)-1,3-dihydro-2H-indol-2-ones (5a-5t)- The 2-indolinone (10 mmol) was dissolved in methanol (100 ml) and treated with appropriate carbaldehyde (**4a-4t**) (10 mmol) and piperidine (1 ml). The reaction mixture was refluxed for 1-5 h

(according to a TLC test), cooled and concentrated under reduced pressure. The resulting precipitate was collected by filtration with a yield of 70-85% and it was purified by recrystallisation from ethanol.

3-((2-benzyl-6-(4-bromophenyl)imidazo[2,1-b][1,3,4]thiadiazol-5-yl)methylidene)-1,3-dihydro-2H-indol-2-one (5a)- Yield 80%. IR 3208, 3095, 3055, 1708, 1613, 1459, 1399, 1202. ¹H-NMR (DMSO-d₆, 400 MHz) δ (ppm): 4.41 (2H, s, CH₂), 6.60-6.69 (2H, m, ar), 6.85 (1H, d, *J* = 8), 7.16-7.20 (1H, m, ar), 7.29-7.37 (5H, m, ar), 7.58-7.60 (3H, dm, *J* = 8), 7.63 (2H, d, *J* = 8), 10.65 (1H, s, NH). -ESI (*m/z*): 515.3 (M-2)

3-((2-benzyl-6-(4-chlorophenyl)imidazo[2,1-b][1,3,4]thiadiazol-5-yl)methylidene)-1,3-dihydro-2H-indol-2-one (5b)- Yield 82%. IR 3187, 3092, 3057, 2962, 1709, 1458, 1400, 1202. ¹H-NMR (DMSO-d₆, 400 MHz) δ (ppm): 4.41 (2H, s, -CH₂-), 6.62 (1H, d, *J* = 8), 6.66 (1H, t, *J* = 16), 6.85 (1H, d, *J* = 8), 7.16-7.20 (1H, m, ar), 7.28-7.38 (5H, m, ar), 7.47 (2H, d, *J* = 8), 7.58 (1H, s, ar), 7.70 (2H, d, *J* = 8), 10.65 (1H, s, NH). +ESI (*m/z*): 467.6 (M+1).

3-((2-benzyl-6-(4-methoxyphenyl)imidazo[2,1-b][1,3,4]thiadiazol-5-yl)methylidene)-1,3-dihydro-2H-indol-2-one (5c)- Yield 79%. IR 3172, 3091, 2950, 1709, 1611, 1462, 1410, 1210. ¹H-NMR (DMSO-d₆, 400 MHz) δ (ppm): 3.84 (3H, s, OCH₃), 4.41 (2H, s, -CH₂-), 6.65-6.68 (2H, m, ar), 6.85 (1H, d, *J* = 8), 7.14-7.19 (2H, m, ar), 7.29-7.35 (6H, m, ar), 7.57 (1H, s, =CH-), 7.61-7.63 (1H, m, ar), 7.88-7.89 (1H, m, ar), 10.64 (1H, s, NH). -ESI (*m/z*): 465.3 (M-1).

3-((2-(4-chlorobenzyl)-6-phenyl)imidazo[2,1-b][1,3,4]thiadiazol-5-yl)methylidene)-1,3-dihydro-2H-indol-2-one (5e)- Yield 81%. IR 3226, 3091, 2895, 1703, 1615, 1461, 1209. ¹H-NMR (DMSO-d₆, 400 MHz) δ (ppm): 4.44 (2H, s, CH₂), 6.62-6.68 (2H, m, ar), 6.86 (1H, d, *J* = 8), 7.17-7.19 (1H, m, ar), 7.35-7.45 (8H, m, ar), 7.60 (1H, s, =CH-), 7.72 (1H, d, *J* = 8), 10.65 (1H, s, NH). -ESI (*m/z*): 469.5 (M-1).

3-((2-(4-chlorobenzyl)-6-(4-chlorophenyl)imidazo[2,1-b][1,3,4]thiadiazol-5-yl)methylidene)-1,3-dihydro-2H-indol-2-one (5f)- Yield 83%. IR 3172, 3089, 3037, 2959, 1708, 1612, 1457, 1203. ¹H-NMR (DMSO-d₆, 400 MHz) δ (ppm): 4.40 (2H, s, -CH₂-), 6.65-6.69 (2H, m, ar), 6.85 (1H, d, *J* = 8), 7.18 (1H, t, *J* = 16), 7.24 (2H, d, *J* = 8), 7.28-7.37 (4H, m, ar), 7.56 (1H, s, =CH-), 7.60 (2H, d, *J* = 8), 10.63 (1H, s, NH).

3-((2-(4-chlorobenzyl)-6-tolylimidazo[2,1-b][1,3,4]thiadiazol-5-yl)methylidene)-1,3-dihydro-2H-indol-2-one (5g)- Yield 82%. IR 3168, 3089, 2953, 1703, 1617, 1460, 1414, 1204. ¹H-NMR (DMSO-d₆, 400 MHz) δ (ppm): 2.30 (3H, s, -CH₃), 4.41 (2H, s, -CH₂-), 6.62-6.67 (2H, m, ar), 6.85 (1H, d, *J* = 8), 7.15-7.18 (1H, m, ar), 7.24 (2H, d, *J* = 8), 7.33-7.42 (4H, m, ar), 7.54 (1H, s, =CH-), 7.60 (2H, d, *J* = 8), 10.62 (1H, s, NH). -ESI (*m/z*): 483.5 (M-1).

3-((2-benzyl-6-(4-fluorophenyl)imidazo[2,1-b][1,3,4]thiadiazol-5-yl)

-methylidene)-1,3-dihydro-2H-indol-2-one (5i)- Yield 82%. IR 3252, 3187, 3093, 2897, 2824, 1703, 1614, 1499, 1461, 1413, 1224. ¹H-NMR (DMSO-d₆, 400 MHz) δ (ppm): 4.41 (2H, s, -CH₂-), 6.62-6.66 (2H, m, ar), 6.84 (1H, d, *J* = 8), 7.17-7.19 (2H, m, ar), 7.24 (2H, t, *J* = 16), 7.34-7.36 (4H, m, ar), 7.58 (1H, s, ar), 7.70-7.74 (2H, dd, *J* = 8, 8), 10.64 (1H, s, NH).

3-((2-benzyl-6-phenylimidazo[2,1-b][1,3,4]thiadiazol-5-yl)

methylidene)-1,3-dihydro-2H-indol-2-one (5j)- Yield 78%. IR 3184, 3068, 2895, 2823, 1702, 1616, 1458, 1335, 1208. ¹H-NMR (DMSO-d₆, 400 MHz) δ (ppm): 4.41 (2H, s, -CH₂-), 6.63-6.67 (2H, m, ar), 6.85 (1H, d, *J* = 8 Hz), 7.17-7.19 (1H, m, ar), 7.30-7.36 (6H, m, ar), 7.41 (2H, t, *J* = 16), 7.59 (1H, s, ar), 7.71 (2H, d, *J* = 8), 10.64 (1H, s, NH). -ESI (*m/z*): 435.5 (M-1)

3-((2-(4-chlorobenzyl)-6-(4-nitrophenyl)imidazo[2,1-b][1,3,4]

-thiadiazol-5-yl)methylidene)-1,3-dihydro-2H-indol-2-one (5l)- Yield 81%. IR 3148, 3075, 2835, 1708, 1641, 1606, 1464, 1415, 1342, 1226. ¹H-NMR (DMSO-d₆, 400 MHz) δ (ppm): 4.46 (2H, s, -CH₂-), 6.59 (1H, d, *J* = 8), 6.66 (1H, t, *J* = 8), 6.87 (1H, d, *J* = 8), 7.19 (1H, t, *J* = 16), 7.36-7.42 (4H, m, ar), 7.64 (1H, s, =CH-), 7.99 (2H, d, *J* = 8), 8.26 (2H, d, *J* = 8), 10.71 (1H, s, NH).

3-((2-(4-chlorobenzyl)-6-(4-bromophenyl)imidazo[2,1-b][1,3,4]

-thiadiazol-5-yl)methylidene)-1,3-dihydro-2H-indol-2-one (5m)- Yield 85%. IR 3144, 3080, 2888, 2821, 1705, 1618, 1487, 1461, 1403, 1209. ¹H-NMR (DMSO-d₆, 400 MHz) δ (ppm): 4.45 (2H, s, -CH₂-), 6.62 (1H, d, *J* = 8), 6.68 (1H, t, *J* = 16), 6.87 (1H, d, *J* = 8), 7.20 (1H, t, *J* = 16), 7.36-7.44 (4H, m, ar), 7.58 (1H, s, =CH-), 7.63 (2H, d, *J* = 8), 7.65 (2H, d, *J* = 8), 10.67 (1H, s, NH). -ESI (*m/z*): 549.5 (M-1).

3-((2-(4-chlorobenzyl)-6-(4-fluorophenyl)imidazo[2,1-b][1,3,4]

-thiadiazol-5-yl)methylidene)-1,3-dihydro-2H-indol-2-one (5n)- Yield 80%. IR 3168, 3092, 2897, 2825, 1704, 1616, 1496, 1462, 1413, 1222. ¹H-NMR (DMSO-d₆, 400 MHz) δ (ppm): 4.45 (2H, s, -CH₂-), 6.62 (1H, d, *J* = 8), 6.67 (1H, t, *J* = 16), 6.86 (1H, d, *J* = 8), 7.19 (1H, t, *J* = 16), 7.26 (2H, t, *J* = 16), 7.36-7.44 (4H, m, ar), 7.59 (1H, s, =CH-), 7.73-7.76 (2H, m, ar), 10.65 (s, 1H, NH).

3-((2-(4-chlorobenzyl)-6-(2-oxo-2H-chromen-3-yl)imidazo[2,1-b][1,3,4]thiadiazol-5-yl)

methylidene)-1,3-dihydro-2H-indol-2-one (5o)- Yield 83%. IR 3136, 3071, 2898, 2836, 1748, 1702, 1618, 1469, 1220. ¹H-NMR (DMSO-d₆, 400 MHz) δ (ppm): 4.47 (2H, s, -CH₂-), 6.61 (2H, d, *J* = 8), 6.83 (1H, d, *J* = 8), 7.12-7.16 (1H, m, ar), 7.36-7.43 (6H, dd, *J* = 8, 8), 7.63 (1H, t, *J* = 16), 7.75 (1H, s, =CH-), 7.87 (1H, d, *J* = 8), 8.51 (1H, s, ar), 10.59 (1H, s, NH). -ESI (*m/z*): 537.7 (M-1).

3-[[6-(4-chlorophenyl)-2-methylimidazo[2,1-b][1,3,4]thiadiazol-5-yl] methylidene)-1,3-dihydro-2H-indol-2-one (5p)- Yield 80%. IR 3150, 3066, 2899, 1750, 1700, 1621, 1471, 1221. ¹H-NMR (DMSO-d₆, 400 MHz) δ (ppm): 2.71 (3H, s, CH₃), 6.61 (1H, d, *J* = 8 Hz), 6.66 (1H, t, *J* = 16), 6.83 (1H, d, *J* = 8), 7.15 (1H, t, *J* = 16), 7.46 (2H, d, *J* = 8), 7.58 (1H, s, -CH=), 7.69 (2H, d, *J* = 8), 10.63 (1H, s, NH). ESI (*m/z*): 393.1 (M).

3-[[6-(4-bromophenyl)-2-methylimidazo[2,1-b][1,3,4]thiadiazol-5-yl)methylidene]-1,3-dihydro-2H-indol-2-one (5q)- Yield 75%. IR 3126, 3071, 2892, 2830, 1745, 1698, 1618, 1458, 1227. ¹H-NMR (DMSO-d₆, 400 MHz) δ (ppm): ¹H-NMR (DMSO-d₆, 400 MHz) δ (ppm): 2.71 (3H, s, CH₃), 6.61 (1H, d, *J* = 8), 6.67 (1H, t, *J* = 16), 6.83 (1H, d, *J* = 8), 7.15 (1H, t, *J* = 16), 7.57 (1H, s, =CH-), 7.59 (2H, d, *J* = 8), 7.65 (2H, d, *J* = 8), 10.64 (1H, s, NH). ESI (*m/z*): 437.1 (M).

3-[[6-(4-nitrophenyl)-2-methylimidazo[2,1-b][1,3,4]thiadiazol-5-yl)methylidene]-1,3-dihydro-2H-indol-2-one (5r)- Yield 78%. IR 3129, 3068, 2895, 2841, 1751, 1706, 1625, 1469, 1224. ¹H-NMR (DMSO-d₆, 400 MHz) δ (ppm): 2.72 (3H, s, CH₃), 6.58 (1H, d, *J* = 8), 6.64 (1H, t, *J* = 16), 6.84 (1H, d, *J* = 8), 7.15 (1H, t, *J* = 16), 7.64 (1H, s, =CH-), 7.97 (2H, d, *J* = 8), 8.25 (2H, d, *J* = 8), 10.68 (1H, s, NH). -ESI (*m/z*): 402.1 (M-2).

3-[[6-(4-methylphenyl)-2-methylimidazo[2,1-b][1,3,4]thiadiazol-5-yl)methylidene]-1,3-dihydro-2H-indol-2-one (5s)- Yield 81%. IR 3133, 3080, 2899, 2841, 1751, 1709, 1618, 1475, 1223. ¹H-NMR (DMSO-d₆, 400 MHz) δ (ppm): 2.29 (3H, s, CH₃), 2.69 (3H, s, CH₃), 6.66 (1H, d, *J* = 8), 6.69 (1H, t, *J* = 16), 6.83 (1H, d, *J* = 8), 7.15 (1H, t, *J* = 16), 7.23 (2H, d, *J* = 8), 7.56 (1H, s, =CH-), 7.60 (2H, d, *J* = 8), 10.61 (1H, s, NH). +ESI (*m/z*): 373.1 (M+1).

3-[[6-(4-methoxyphenyl)-2-methylimidazo[2,1-b][1,3,4]thiadiazol-5-yl)methylidene]-1,3-dihydro-2H-indol-2-one (5t)- Yield 80%. IR 3121, 3065, 2892, 2835, 1747, 1700, 1619, 1465, 1218. ¹H-NMR (DMSO-d₆, 400 MHz) δ (ppm): 2.69 (3H, s, CH₃), 3.75 (3H, s, OCH₃), 6.71-6.65 (2H, m, ar), 6.83 (1H, d, *J* = 8), 6.99 (2H, d, *J* = 8), 7.14 (1H, t, *J* = 16), 7.56 (1H, s, =CH-), 7.64 (2H, d, *J* = 8), 10.60 (1H, s, NH). -ESI (*m/z*): 387.1 (M-1).

Biology

Enzymes, chemicals, and reagents- Chemical reagents were obtained from Sigma Chemical Co. (USA), Amresco (USA) and SRL (India). DNA modifying enzymes were from New England Biolabs (USA) and Fermentas (USA). Antibodies were purchased as specified. Culture media were from Sera Laboratory International limited (UK), FBS and PenStrep were from Gibco BRL (USA). HA 14-1, Gossypol and Epigallocatechin were purchased from SantaCruz Biotechnology, USA.

Cell lines and culture- K562 (human chronic myelogenous leukemia), T47D (human breast cancer), 293T (human embryonic kidney epithelial cell line) and EAC (mouse breast cancer) were purchased from National Centre for Cell Science, Pune, India. A2780 (ovarian cancer) was purchased from ATCC, USA. CEM (T-cell leukemia), NALM6 (B-cell leukemia) and REH (B-cell leukemia) were kind gifts from Dr. M.R. Lieber, USA. HeLa (human cervical carcinoma), P388D1 (mouse lymphoma), LNCaP (human prostate carcinoma) and Molt4 (T-cell leukemia) were purchased from National Centre for Cell Science, Pune, India. Cells were cultured in RPMI 1640 or DMEM medium supplemented with 10% fetal bovine serum (FBS), 100 µg/ml Penicillin, and 100 µg streptomycin/ml and incubated at 37°C in a humidified atmosphere containing 5% CO₂.

Plasmid constructs- Codon optimized BCL2 cDNA was commercially synthesized for expression in *E. coli* (Life Technologies, USA). Transmembrane deleted codon optimized BCL2 was amplified using primers SV29 and SV30, products were digested with BamHI and XhoI, and cloned into respective sites of pET28a to generate pMS42. DNA sequence corresponding to the BH1 domain of BCL2 was deleted by employing site directed mutagenesis, using primers SV35 and SV36 to generate pMS45. Similarly, pMS46 containing BH3 deleted BCL2 was obtained (using SV37 and SV38 primers). Amplicons were treated with KLD mix (New England Biolabs, USA) and transformed into *E. coli* to generate the constructs. In all cases, sequence of the cloned amplicon was confirmed by DNA sequencing.

pMS8 vector, for bacterial overexpression and purification of N terminal His-tagged BCL2, was generated by amplifying the *BCL2* coding sequence using primers MS50 and MS51. The PCR product, which is truncated version of BCL2 (terminal 69 amino acids truncation including transmembrane and a part of BH2 domain), was gel purified and cloned into NdeI and XhoI site of pET28a+ to obtain the pMS8 plasmid. The identity of clone was confirmed by restriction digestion followed by sequencing.

Truncated BAK lacking transmembrane domain was PCR amplified from human cDNA using the primers SS107 and SS109. The amplified product was cloned into EcoRI and HindIII sites of pETDuet-1 vector. The resulting clone, pMS27, was used for expression studies following sequence confirmation.

BCL2A1 plasmid was a gift from Nicola Burgess Brown (Addgene plasmid # 42399). For mammalian expression, BCL2A1 plasmid was digested using KpnI and EcoRI, and cloned into pCDNA3-mRFP. BCL-xL plasmid was a gift from Dr. J. Lakey, UK. pETDuet-1 was a gift from Dr. B Gopal, India. pCDNA3.1-hMcl-1 was a gift from Roger Davis (Addgene plasmid # 25375).

Oligomers- Oligomers were designed and synthesized from IDT, USA and Xcelris, India. Oligomers used in the present study were, SV29, 5'-GGATCCATGGCACATGCAGG-3'; SV30, 5'-CTCGAGTTAATCAAACAGCG-3'; SV35, 5'-ACACATAACACCTTCAACAACGGTTGCA-3'; SV36, 5'-CGTTGTTGAAGGTGTTATGTGTG-TGGAA-3'; SV37, 5'-ACGACGATAAA-CAGGCGGAACCGGACTC-3'; SV38, 5'-CCGCCTGTTTATCGTCGTGATTTTGCA-3'; MS50, 5'-CATATGATGGCGCACGCTGGGAG-3'; MS51, 5'-CTCGAGTCAGGGCGACATCTC-CC-3'; SS107, 5'-GAATTCATGGCTTCGGGG-CAAG-3'; SS109, 5'-AAGCTTATTGCCCAAGT-TCAG-3'; SV74, 5'-GTGTCAAAGTCCCCTC-AGGA-3'; SV75, 5'-ACACAGCTCACC-TCTTTCTGT-3'; SV76, 5'-CTGCAGTG-CGTCCTACAGAT-3'; SV77, 5' TTCTGGC-AGTGTCTACGGAC 3'.

In silico docking- The 2D structures of the synthesized compounds were built and subsequently converted to 3D structures using Discovery studio 2.5 and optimized using steepest-descent algorithm available within the same package (Discovery Studio 2.5). Crystal structure of human BCL2 (1GJH) retrieved from PDB database was used to dock the synthesized compounds with the aid of AutoDock Vina [26]. Input files for AutoDock Vina were prepared using AutoDock Tools 4.2 that included

addition of polar hydrogen atoms and gasteiger charges [45]. Autogrid 4.2 was used to generate the grid map. A grid box of size 40×40×40 Å³ with a grid spacing of 0.375 Å was set to cover the putative binding site of the BCL2. Docking was performed keeping BCL2 fixed while the inhibitors were allowed to flex. 40 conformations were generated for each inhibitor. All other parameters were set to default values. PyMOL 1.7 was used to visualize the results obtained by Vina. Conformation pertaining to lowest binding energy was chosen for further studies. MCL1 structure in which BH1 domain is swapped with that of BCL2 was modelled (2MHS; 4OQ6; 1WSX; 1GJH as templates) using MODELER 9v7 available within the Discovery studio 2.5 package. Subsequently, the model was energy-minimized using Sander module of AMBER 14.0 (ff14SB) (Case,D.A., Babin, V., Berryman, JT., Betz, RM., Cai, Q., Cerutti, DS.,et al. (2014), AMBER 14, University of California, San Francisco). Superposition of wild-type MCL1 and BH1 domain swapped MCL1 model displayed a RMSD of ~0.4 Å (data not shown). Interaction between various BCL2 family proteins and Disarib was deciphered using the graphical interface of insight II³ on an O2 sgi workstation. Figures were prepared using PyMOL (<http://www.pymol.org>).

Trypan blue exclusion assay- Cell viability after treatment with the potential BCL2 inhibitors was assayed using trypan blue exclusion assay [46, 47]. Briefly, the compounds (10, 50, 100 and 250 μM) were added to the cells (NALM6, K562 and CEM) and were harvested at 48 h post treatment. Number of viable cells was ascertained by mixing cells with equal volume of 0.4% trypan blue stain (Sigma Aldrich). The cells were then counted using a haemocytometer and the cell number was plotted against time period of cell growth. Data from the 48 h time point was used for calculating the IC₅₀ value of individual compound from selected cell lines.

In experiments wherein cytotoxicity induced by Disarib was compared in REH, K562, NALM6, 293T, CEM and T47D, cells were treated with 2, 5, 10 and 20 μM of Disarib. DMSO treated cells served as the vehicle control. Cell viability was assayed after 48 and 72 h of the compound treatment by trypan blue assay. Results shown are derived from a minimum of three independent experiments.

MTT assay- In order to measure cell proliferation after treatment with the compounds, the cultured cells (NALM6, K562 and CEM; 25,000 cells/ml) were treated with different concentrations (10, 50, 100 and 250 μM) of the compounds. Equal volume of cells (100 μl) were collected at the end of 48 h and 72 h and incubated with MTT reagent (Sigma Aldrich) at 5 mg/ml concentration (at 37°C for 2 h) as described [48, 49]. Change in the intensity of color was measured at 570 nm. IC₅₀ values were calculated using data from 48 h time points.

Knockdown and overexpression of BCL2- NALM6 cells resuspended in serum free medium were transfected with *BCL2* siRNA (50, 100 and 250 nM; Cat. No. S100299397, Qiagen) using oligofectamine (Invitrogen, USA), following the manufacturer's instructions. The cells were grown in serum free medium for 6 h, after which the culture was supplemented with 10% FBS. The cells were then harvested, lysed in RIPA buffer and the lysates were checked by immunoblotting for BCL2

expression levels. For experiments in which cells were treated with Disarib, NALM6 cells were treated with either 250 nM BCL2 siRNA or 250 nM scrambled siRNA (Cat. No. D-001210-01-05, Dharmacon). The cells were grown in serum free medium for 6 h, then supplemented with 10% FBS and allowed to grow for 24 h and exposed to Disarib (5 and 10 μ M). The cell viability was determined by trypan blue assay as described above.

For restoration of BCL2 expression following knockdown by siRNA, NALM6 cells were transfected with 25 μ g of BCL2 overexpression vector (*BCL2*-PCMV SPORT) using lipofectamine (Invitrogen, USA) as per manufacturer's protocol. After 6 h of growth in serum free medium, the cells were supplemented with 10% FBS and were grown for an additional 24 h before treatment with Disarib (5 μ M). Cytotoxicity assays to measure cell viability were carried out after 48 h of compound treatment. Overexpression of MCL1 and BCL2A1 was performed using PEI (polyethylimine) method of transfection in NALM6 cells. In brief, ~5 lakh cells were transfected with 5 μ g of plasmid (pCDNA3.1-hMcl-1 for MCL1 and pMH1 for BCL2A1) and 10 μ g PEI, and mixed in OptiMEM medium (GIBCO, USA). The solution was then added to the cells, and incubated at 37°C for a period of 48 h. Cells were harvested, RNA was isolated, and cDNA was prepared subsequently as described [47]. The cDNA was then subjected to RT-PCR analysis using specific primers against MCL1 and BCL2A1 genes.

Evaluation of effect of Disarib on primary cells derived from chronic lymphocytic leukemic patients-

The use of primary CLL cells from consenting patients had approval from the Liverpool Research Ethics Committee. The cytotoxicity of Disarib against primary leukemic samples was assayed as described earlier [50]. Briefly, 6 chronic lymphocytic leukemia (CLL) patient samples were incubated with Disarib (0, 1, 3 and 10 μ M) for 4 h after which the cells were collected and assayed for initiation of apoptosis by Annexin V FITC binding and FACS assessment. Data from multiple experiments is represented as % apoptosis observed above levels of spontaneous apoptosis in DMSO treated controls. Error bars indicate mean \pm SEM.

Overexpression and purification of BCL2 (wild type and mutants), BAK, BCL-xL and BCL2A1- The transmembrane deleted versions of BCL2, BCL-xL, BAK, BCL2, BCL2 (delta-BH1), BCL2 (delta-BH3) and BCL2A1 were overexpressed in *E. coli*, BL21 pLysS. For purification of wild type BCL2 protein (variant 2 [51]), cells transformed with pMS42 was cultured in LB medium (1L) containing ampicillin (100 μ g/ml) and chloramphenicol (34 μ g/ml). A transmembrane deleted version was used, to facilitate the BCL2 purification. The cells were induced with 1 mM IPTG overnight at 16°C, harvested and resuspended in lysis buffer (20 mM Tris-HCl [pH 8.0], 50 mM NaCl, 5% glycerol, 1% Triton X-100 and 1 mM PMSF). The cells were then sonicated, centrifuged and clarified extract was then loaded onto Ni-NTA column (Novagen). Protein was eluted with increasing concentration of imidazole (100 mM-400 mM). Fractions were analysed on a 12% SDS PAGE followed by CBB staining. BCL2 enriched fractions were pooled and dialyzed against dialysis buffer (PBS containing 0.05% Triton X-100, 1 mM beta-mercaptoethanol, 5 % glycerol and 0.1 mM PMSF) overnight at 4°C.

The dialyzed fraction was loaded onto an anion exchange column Uno-sphere Q (BioRad), and the protein was eluted in buffer containing 50 mM Tris-HCl (pH 8.0), 250 mM NaCl, 5 mM DTT, 0.1% Triton X-100, 5% glycerol and 1 mM PMSF, with increasing concentration of NaCl (150-300 mM). Fractions were analysed on a 12% SDS PAGE followed by CBB staining and those containing nearly homogenous BCL2 were pooled and stored at -80°C. Purity and identity of the protein was confirmed by silver staining and immunoblotting.

For BCL2 (delta-BH1) and BCL2 (delta-BH3), bacterial cells transformed with pMS45 and pMS46, respectively, were cultured in LB medium containing ampicillin (100 µg/ml) and chloramphenicol (34 µg/ml). Both the proteins were overexpressed and purified as described above.

For purification of truncated version of BCL2, pMS8 was cultured in LB medium (1 L) in presence of appropriate antibiotics. The cells were induced with 0.5 mM IPTG overnight at 16°C, harvested, resuspended in lysis buffer (50 mM Tris-HCl [pH 8.0], 50 mM NaCl, 5% glycerol, 1% Triton X-100 and 1 mM PMSF) and sonicated. The clarified lysate was loaded onto Ni-NTA column (Novagen) and protein was eluted according to manufacturer's instructions. Fractions were analysed on 12% SDS-PAGE and BCL2 enriched fractions were pooled and loaded onto UNO sphere Q anion exchange column (BioRad). Proteins were eluted with an increasing gradient of NaCl (200-500 mM) and analysed. Fractions of interest were further pooled and loaded onto a size exclusion column, Biogel P100 (BioRad). Protein elution was done with a buffer containing 50 mM Tris-HCl (pH 8.0), 250 mM NaCl, 5 mM DTT, 0.1% Triton X-100, 5% glycerol and 1 mM PMSF, and analysed on a SDS-PAGE by silver staining. The fractions nearly homogenous for BCL2 were pooled, aliquoted and stored at -80°C. Identity and purity of the protein was confirmed by silver staining and immunoblotting.

BCL-xL was overexpressed and purified using the vector pTOLT-BCL-X_L as described earlier [52]. Briefly, the plasmid was transformed into *E. coli*, BL21 pLysS and cultured in LB medium (100 ml) containing ampicillin (100 µg/ml). The culture was induced with 0.5 mM IPTG at 37°C for 3 h. The bacteria were lysed in 20 mM sodium phosphate buffer (pH 8) containing 300 mM NaCl and 1 mM PMSF. The lysate was clarified and BCL-xL was purified using Ni-NTA chromatography as described above. BCL-xL containing fractions were pooled and dialysed against storage buffer (50 mM sodium phosphate buffer [pH 8.0], 300 mM NaCl, 1 mM PMSF, 10% glycerol) and aliquots were stored at -80°C.

For purification of BAK, pMS27 was transformed into *E. coli* BL21 pLysS, grown in LB medium (1 L) containing ampicillin (100 µg/ml), induced with 0.5 mM IPTG at 16°C for 18 h. Protein was purified using a Ni-NTA column as described for BCL2. Elution was performed with a step gradient using 60-800 mM imidazole and the fractions were analysed on 12% SDS PAGE followed by silver staining. BAK containing fractions were pooled and subjected to anion exchange chromatography as described above. Eluted fractions were analysed by silver staining and fractions

with 90% homogeneity of the BAK (250 mM NaCl) were dialysed (20 mM Tris-HCl [pH 8.0], 300 mM NaCl, 1 mM PMSF and 10% glycerol) and stored as aliquots at -80°C .

For BCL2A1 purification, *E. coli* BL21 cells were cultured in LB medium containing ampicillin (100 $\mu\text{g}/\mu\text{l}$). The cells were induced using 1 mM IPTG overnight at 16°C , harvested and resuspended in lysis buffer (20 mM Tris-HCl [pH 8.0], 50 mM NaCl, 5% glycerol, 1% Triton X-100 and 1 mM PMSF). The cells were then sonicated and the clarified lysate was loaded onto Ni-NTA column (Novagen), and the protein was eluted with increasing concentration of imidazole (100 mM-400 mM). Fractions were analysed on a 12% SDS PAGE by CBB staining, and BCL2A1 enriched fractions were pooled and dialyzed against dialysis buffer (PBS containing 0.05% Triton X-100, 1 mM beta-mercaptoethanol, 5 % glycerol and 0.1 mM PMSF) overnight at 4°C and stored at -80°C , till use.

Circular Dichroism (CD)- Circular Dichroism studies were done using purified recombinant BCL2 and BCL-xL in the presence of Disarib, to assess binding as described [53]. The purified proteins (9 μM) were subjected to CD following dilution in PBS and the spectrum was recorded between wavelengths 200 and 250 nm (5 cycles, scan speed of 50 nm/sec at 4°C) in a JASCO J-810 spectropolarimeter. A titration of Disarib was performed with BCL2 at 10, 50, 75, 100 and 150 nM concentrations. Comparative studies of binding were done with 0.5 μM Disarib and BCL2 (9 μM), BCL2 truncated version (6 μM), BAK (8 μM) and BCL-xL (6 μM) under the given conditions. Spectra resulting from buffer alone and buffer containing DMSO equivalent to the inhibitor volumes were subtracted from the protein spectra.

Fluorescence based thermal shift assay- A fluorescence microplate reader (iQ5, BioRad iCycler Multicolor Real-Time PCR detection system) was used to monitor protein unfolding as a function of temperature. The detection involves increase in fluorescence of a fluorophore SYPRO Orange (Sigma, S5692) upon binding to the hydrophobic regions of the gradually unfolded protein. Protein samples (1 μM) were mixed with HEPES buffer (10 mM, pH 7.4) consisting of 1x SYPRO orange dye and appropriate concentrations of ligand over the range of several folds, and were incubated in 96-well PCR microplates (BioRad) in the RT-PCR device [27, 28].

Ligand concentrations were varied between 5 nM to 100 μM and the concentration of DMSO was kept constant at 2% throughout the screens. Samples were heated at 0.5°C per minute, ranging from 10°C to 95°C and the fluorescence intensity was measured at interval of 0.5°C [27]. Cy5 filter with red-orange color intensity was selected for the SYPRO Orange detection. All the experiments were done in triplicates and the average (or best two) was considered during the analysis. Appropriate buffer blanks were subtracted for the same in each set.

Fluorescence intensities were plotted as a function of temperature using GraphPad Prism software and the melting temperature of protein was determined for individual ligand concentrations (using sigmoidal dose response function of GraphPad). The net change in T_m was then plotted against increasing ligand concentration. The dissociation constants were determined by analysing the data

under non-linear regression (curve fit) model (least square ordinary fit) using the Binding Saturation 'one site-specific binding' function.

Immunoblotting- Immunoblotting was performed with 40 µg of NALM6 cell lysates or as specified. [54, 55]. The cell lysates were resolved on 8-12% SDS PAGE gels and transferred onto PVDF membrane (Millipore, USA). The blots were blocked with 5% skim milk in 0.1% PBST and incubated with primary antibodies- BCL2, TUBULIN, Caspase 8 (Santa Cruz Biotechnology, USA), activated Caspase 3 and activated Caspase 9 (Cell Signalling Technology, USA). After incubation with appropriate secondary antibodies (1:10,000 in 0.1% PBST; Santa Cruz Biotechnology, USA), the blots were developed using enhanced chemiluminescence substrate (Immobilon™ western, Millipore, USA) and the images were captured by LAS 3000 (FUJI, JAPAN) gel documentation system. Lysates prepared for experiments involving coimmunoprecipitation (nondenaturing method), BCL2 knockdown, over expression and to check the expression of different proteins in different cell lines (RIPA buffer method) were analysed in a similar manner. For recombinant protein validation and purified protein coimmunoprecipitation experiments, 2.5 µg protein was analysed under similar conditions.

Annexin-FITC/PI staining- To check the mode of cell death induced by the Disarib, annexin-FITC/PI staining was carried out as described previously [56, 57]. Briefly, Molt4 cells (0.25×10^5 cells) were treated with Disarib (0, 1, 2 and 5 µM) for 48 h. DMSO treated cells were used as control. Cells were processed, stained with annexin-FITC/PI and subjected to FACS analysis. Results were analysed in Flowing software (version2.5) with minimum of 10,000 cells and plotted as dot plots. Cells which were positive for annexin-FITC/PI staining were calculated and presented as bar diagram with error bars.

Hoechst staining- Molt4 cells were assessed for nuclear condensation following Disarib treatment (1 and 2 µM, 48 h) following staining with Hoechst (Hoechst 33342, 1 µM). Images were captured using Zeiss Apotome Microscope under 10X and 40X magnification. ~300 to 500 cells were analyzed from each group and the quantification represented as a table showing percentage condensed cells in each group.

Animal experiments

Animals- Swiss albino mice (4-8 weeks old, female), were purchased from central animal facility, Indian Institute of Science, Bangalore, India and were maintained as per the guidelines of the animal ethical committee in accordance with Indian National Law on animal care and use. The animals were housed in polypropylene cages and provided standard pellet diet (Agro Corporation Pvt. Ltd., Bangalore, India) and water ad libitum. The standard pellet diet is composed of 21% protein, 5% lipids, 4% crude fiber, 8% ash, 1% calcium, 0.6% phosphorus, 3.4% glucose, 2% vitamin, and 55% nitrogen-free extract (carbohydrates). The animals were maintained under controlled conditions of temperature and humidity with a 12 h light/dark cycle.

DLA tumor mouse model- Dalton lymphoma ascitic (DLA) cells were used for developing DLA liquid tumor in Swiss albino mice [33, 46, 47]. Animals were given intraperitoneal injection of DLA cells (0.25×10^6 cells/ mouse) for developing DLA liquid tumor. The mice were then randomly segregated into five groups of which one group served as the tumor control (n=8) and received only the methyl cellulose solution where the compounds were dissolved, while the other groups (in each case n=8) were given intraperitoneal Disarib/ Gossypol/ Epigallocatechin/ HA14-1(10 mg/kg) administration. The first dose of treatment was given on the day of DLA injection, and a total of six doses were administered every alternate day in all the cases. Tumor progression was measured by monitoring the body weight of the animals over a period of 20 days and data obtained is presented with error bars. Further, body weight measurements were recorded in Disarib treated mice (10 mg/kg, every alternate day), and compared with those in untreated control group (n=10 in each group).

Statistical analysis- For each experiment, student's t-test (two tailed), using GraphPad prism (Version 5.1), was employed to calculate the statistical significance of the results reported. Values with p-value less than 0.05 were considered significant. Values are presented as mean \pm SEM.

Acknowledgements

We thank Prof N. Yathindra for his help in *in silico* studies, M. Nambiar,

for help during initial stages of the study, Prof R. Manjunath for support. We also thank M. Pandey, M. Nambiar and SCR lab members for critical reading of the manuscript. BCL-xL plasmid was a gift from Jeremy Lakey (UK). pETDuet-1 was from B Gopal (India). We thank NMR, Mass Spectrometry (MBU) at IISc. Financial assistance from Leukemia Research Foundation, USA and from IISc-DBT partnership programme [DBT/BF/PR/INS/2011-12/IISc] and the Council of Scientific and Industrial Research (37(1579)/13/EMR-II) for SCR and All India Council for Technical Education, New Delhi (Ref. No. 8023/BOR/RID/RPS-169/2008-09) for SSK are acknowledged. AS is a Bhatnagar Fellow of the Council of Scientific and Industrial Research (CSIR), India. DI and SV are supported by IISc fellowship, GG by DeitY, Government of India (India) and Department of IT, BT and S&T, Government of Karnataka, India.

Conflict of interest

An Indian Patent application on the "Design, synthesis and characterization of BCL2 inhibitors targeting the BH1 domain of BCL2", has been filed.

Author contributions

SCR, SSK, AS, DI, SV and GG conceived and designed the experiments. DI, SV, AM, GG, SK, MS, MH, VG, MG, MV and BC performed the experiments. SCR, SV, AS, SSK, DI, NK, GG and BC interpreted the data and wrote the manuscript.

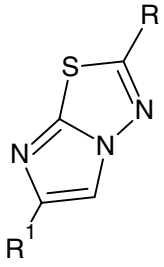
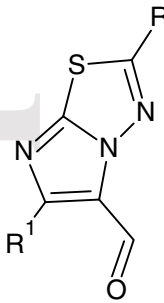
REFERENCES

1. Cotter, T. G. (2009) Apoptosis and cancer: the genesis of a research field, *Nat Rev Cancer*. **9**, 501-7.
2. Ferri, K. F. & Kroemer, G. (2001) Organelle-specific initiation of cell death pathways, *Nat Cell Biol*. **3**, E255-63.
3. Willis, S. N., Fletcher, J. I., Kaufmann, T., van Delft, M. F., Chen, L., Czabotar, P. E., Ierino, H., Lee, E. F., Fairlie, W. D., Bouillet, P., Strasser, A., Kluck, R. M., Adams, J. M. & Huang, D. C. (2007) Apoptosis initiated when BH3 ligands engage multiple Bcl-2 homologs, not Bax or Bak, *Science*. **315**, 856-9.
4. Gross, A., McDonnell, J. M. & Korsmeyer, S. J. (1999) BCL-2 family members and the mitochondria in apoptosis, *Genes Dev*. **13**, 1899-911.
5. Lin, Y., Fukuchi, J., Hiipakka, R. A., Kokontis, J. M. & Xiang, J. (2007) Up-regulation of Bcl-2 is required for the progression of prostate cancer cells from an androgen-dependent to an androgen-independent growth stage, *Cell Res*. **17**, 531-6.
6. Campos, L., Rouault, J. P., Sabido, O., Oriol, P., Roubi, N., Vasselon, C., Archimbaud, E., Magaud, J. P. & Guyotat, D. (1993) High expression of bcl-2 protein in acute myeloid leukemia cells is associated with poor response to chemotherapy, *Blood*. **81**, 3091-6.
7. Kirkin, V., Joos, S. & Zornig, M. (2004) The role of Bcl-2 family members in tumorigenesis, *Biochim Biophys Acta*. **1644**, 229-49.
8. Reed, J. C. (1997) Bcl-2 family proteins: regulators of apoptosis and chemoresistance in hematologic malignancies, *Semin Hematol*. **34**, 9-19.
9. Cho, H. J., Kim, J. K., Kim, K. D., Yoon, H. K., Cho, M. Y., Park, Y. P., Jeon, J. H., Lee, E. S., Byun, S. S., Lim, H. M., Song, E. Y., Lim, J. S., Yoon, D. Y., Lee, H. G. & Choe, Y. K. (2006) Upregulation of Bcl-2 is associated with cisplatin-resistance via inhibition of Bax translocation in human bladder cancer cells, *Cancer Let*. **237**, 56-66.
10. Konopleva, M., Tari, A. M., Estrov, Z., Harris, D., Xie, Z., Zhao, S., Lopez-Berestein, G. & Andreeff, M. (2000) Liposomal Bcl-2 antisense oligonucleotides enhance proliferation, sensitize acute myeloid leukemia to cytosine-arabioside, and induce apoptosis independent of other antiapoptotic proteins, *Blood*. **95**, 3929-38.
11. Gutierrez-Puente, Y., Zapata-Benavides, P., Tari, A. M. & Lopez-Berestein, G. (2002) Bcl-2-related antisense therapy, *Semin Oncol*. **29**, 71-6.
12. Wang, J. L., Zhang, Z. J., Choksi, S., Shan, S., Lu, Z., Croce, C. M., Alnemri, E. S., Korngold, R. & Huang, Z. (2000) Cell permeable Bcl-2 binding peptides: a chemical approach to apoptosis induction in tumor cells, *Cancer Res*. **60**, 1498-502.
13. Shangary, S. & Johnson, D. E. (2002) Peptides derived from BH3 domains of Bcl-2 family members: a comparative analysis of inhibition of Bcl-2, Bcl-x(L) and Bax oligomerization, induction of cytochrome c release, and activation of cell death, *Biochemistry*. **41**, 9485-95.
14. Arkin, M. (2005) Protein-protein interactions and cancer: small molecules going in for the kill, *Curr Opin Chem Biol*. **9**, 317-24.
15. Real, P. J., Cao, Y., Wang, R., Nikolovska-Coleska, Z., Sanz-Ortiz, J., Wang, S. & Fernandez-Luna, J. L. (2004) Breast cancer cells can evade apoptosis-mediated selective killing by a novel small molecule inhibitor of Bcl-2, *Cancer Res*. **64**, 7947-53.
16. van Delft, M. F., Wei, A. H., Mason, K. D., Vandenberg, C. J., Chen, L., Czabotar, P. E., Willis, S. N., Scott, C. L., Day, C. L., Cory, S., Adams, J. M., Roberts, A. W. & Huang, D. C. (2006) The BH3 mimetic ABT-737 targets selective Bcl-2 proteins and efficiently induces apoptosis via Bak/Bax if Mcl-1 is neutralized, *Cancer Cell*. **10**, 389-99.
17. Souers, A. J., Levenson, J. D., Boghaert, E. R., Ackler, S. L., Catron, N. D., Chen, J., Dayton, B. D., Ding, H., Enschede, S. H., Fairbrother, W. J., Huang, D. C., Hymowitz, S. G., Jin, S., Khaw, S. L., Kovar, P. J., Lam, L. T., Lee, J., Maecker, H. L., Marsh, K. C., Mason, K. D., Mitten, M. J., Nimmer, P. M., Oleksijew, A., Park, C. H., Park, C. M., Phillips, D. C., Roberts, A. W., Sampath, D., Seymour, J. F., Smith, M. L., Sullivan, G. M., Tahir, S. K., Tse, C., Wendt, M. D., Xiao, Y., Xue, J. C., Zhang, H., Humerickhouse, R. A., Rosenberg, S. H. & Elmore, S. W. (2013) ABT-199, a potent and selective BCL-2 inhibitor, achieves antitumor activity while sparing platelets, *Nat Med*. **19**, 202-8.
18. Wang, Z., Azmi, A. S., Ahmad, A., Banerjee, S., Wang, S., Sarkar, F. H. & Mohammad, R. M. (2009) TW-37, a small-molecule inhibitor of Bcl-2, inhibits cell growth and induces apoptosis in pancreatic cancer: involvement of Notch-1 signaling pathway, *Cancer Res*. **69**, 2757-65.
19. Zhai, D., Jin, C., Satterthwait, A. C. & Reed, J. C. (2006) Comparison of chemical inhibitors of antiapoptotic Bcl-2-family proteins, *Cell Death Differ*. **13**, 1419-21.
20. Iyer, D. (2013) *Targeted cancer therapy: The role of BCL2 inhibitors*, Studium Press, LLC, Houston, Texas, USA.
21. Beauchard, A., Laborie, H., Rouillard, H., Lozach, O., Ferandin, Y., Le Guevel, R., Guguen-Guillouzo, C., Meijer, L., Besson, T. & Thiery, V. (2009) Synthesis and kinase inhibitory activity of novel substituted indigoids, *Bioorg Med Chem*. **17**, 6257-63.

22. Mologni, L., Rostagno, R., Brussolo, S., Knowles, P. P., Kjaer, S., Murray-Rust, J., Rosso, E., Zambon, A., Scapozza, L., McDonald, N. Q., Lucchini, V. & Gambacorti-Passerini, C. (2010) Synthesis, structure-activity relationship and crystallographic studies of 3-substituted indolin-2-one RET inhibitors, *Bioorg Med Chem.* **18**, 1482-96.
23. Wang, L. L., Li, J. J., Zheng, Z. B., Liu, H. Y., Du, G. J. & Li, S. (2004) Antitumor activities of a novel indolin-2-ketone compound, Z24: more potent inhibition on bFGF-induced angiogenesis and bcl-2 over-expressing cancer cells, *Eur J Pharmacol.* **502**, 1-10.
24. Kumar, T. S., Kari, V., Choudhary, B., Nambiar, M., Akila, T. S. & Raghavan, S. C. (2010) Anti-apoptotic protein BCL2 down-regulates DNA end joining in cancer cells, *The Journal of biological chemistry.* **285**, 32657-70.
25. Lotem, J. & Sachs, L. (1995) Regulation of bcl-2, bcl-XL and bax in the control of apoptosis by hematopoietic cytokines and dexamethasone, *Cell Growth Differ.* **6**, 647-53.
26. Trott, O. & Olson, A. J. (2010) AutoDock Vina: improving the speed and accuracy of docking with a new scoring function, efficient optimization, and multithreading, *J. Comp Chem.* **31**, 455-61.
27. Vedadi, M., Niesen, F. H., Allali-Hassani, A., Fedorov, O. Y., Finerty, P. J., Jr., Wasney, G. A., Yeung, R., Arrowsmith, C., Ball, L. J., Berglund, H., Hui, R., Marsden, B. D., Nordlund, P., Sundstrom, M., Weigelt, J. & Edwards, A. M. (2006) Chemical screening methods to identify ligands that promote protein stability, protein crystallization, and structure determination, *Proc Natl Acad Sci, USA.* **103**, 15835-40.
28. Niesen, F. H., Berglund, H. & Vedadi, M. (2007) The use of differential scanning fluorimetry to detect ligand interactions that promote protein stability, *Nature Protocols.* **2**, 2212-21.
29. Rosen, C. G. & Weber, G. (1969) Dimer formation from 1-amino-8-naphthalenesulfonate catalyzed by bovine serum albumin. A new fluorescent molecule with exceptional binding properties, *Biochemistry.* **8**, 3915-20.
30. Fedorov, O., Marsden, B., Pogacic, V., Rellos, P., Muller, S., Bullock, A. N., Schwaller, J., Sundstrom, M. & Knapp, S. (2007) A systematic interaction map of validated kinase inhibitors with Ser/Thr kinases, *Proc Natl Acad Sci, USA.* **104**, 20523-8.
31. Hanada, M., Delia, D., Aiello, A., Stadtmayer, E. & Reed, J. C. (1993) bcl-2 gene hypomethylation and high-level expression in B-cell chronic lymphocytic leukemia, *Blood.* **82**, 1820-8.
32. Marschitz, I., Tinhofer, I., Hittmair, A., Egle, A., Kos, M. & Greil, R. (2000) Analysis of Bcl-2 protein expression in chronic lymphocytic leukemia. A comparison of three semiquantitation techniques, *Am J Clin Pathol.* **113**, 219-29.
33. Sharma, S., Panjamurthy, K., Choudhary, B., Srivastava, M., Shahabuddin, M., Giri, R., Advirao, G. M. & Raghavan, S. C. (2013) A novel DNA intercalator, 8-methoxy pyrimido[4',5':4,5]thieno (2,3-b)quinoline-4(3H)-one induces apoptosis in cancer cells, inhibits the tumor progression and enhances lifespan in mice with tumor, *Molecular Carcinogen.* **52**, 413-25.
34. Kolluri, S. K., Zhu, X., Zhou, X., Lin, B., Chen, Y., Sun, K., Tian, X., Town, J., Cao, X., Lin, F., Zhai, D., Kitada, S., Luciano, F., O'Donnell, E., Cao, Y., He, F., Lin, J., Reed, J. C., Satterthwait, A. C. & Zhang, X. K. (2008) A short Nur77-derived peptide converts Bcl-2 from a protector to a killer, *Cancer Cell.* **14**, 285-98.
35. Kitada, S., Kress, C. L., Krajewska, M., Jia, L., Pellicchia, M. & Reed, J. C. (2008) Bcl-2 antagonist apogossypol (NSC736630) displays single-agent activity in Bcl-2-transgenic mice and has superior efficacy with less toxicity compared with gossypol (NSC19048), *Blood.* **111**, 3211-9.
36. Oakes, S. R., Vaillant, F., Lim, E., Lee, L., Breslin, K., Feleppa, F., Deb, S., Ritchie, M. E., Takano, E., Ward, T., Fox, S. B., Generali, D., Smyth, G. K., Strasser, A., Huang, D. C., Visvader, J. E. & Lindeman, G. J. (2012) Sensitization of BCL-2-expressing breast tumors to chemotherapy by the BH3 mimetic ABT-737, *Proc Natl Acad Sci, USA.* **109**, 2766-71.
37. Wlodkowic, D., Skommer, J. & Pelkonen, J. (2006) Multiparametric analysis of HA14-1-induced apoptosis in follicular lymphoma cells, *Leuk Res.* **30**, 1187-92.
38. Vaillant, F., Merino, D., Lee, L., Breslin, K., Pal, B., Ritchie, M. E., Smyth, G. K., Christie, M., Phillipson, L. J., Burns, C. J., Mann, G. B., Visvader, J. E. & Lindeman, G. J. (2013) Targeting BCL-2 with the BH3 mimetic ABT-199 in estrogen receptor-positive breast cancer, *Cancer Cell.* **24**, 120-9.
39. Anderson, N. M., Harrold, I., Mansour, M. R., Sanda, T., McKeown, M., Nagykar, N., Bradner, J. E., Lan Zhang, G., Look, A. T. & Feng, H. (2014) BCL2-specific inhibitor ABT-199 synergizes strongly with cytarabine against the early immature LOUCY cell line but not more-differentiated T-ALL cell lines, *Leukemia.* **28**, 1145-8.
40. Pan, R., Hogdal, L. J., Benito, J. M., Bucci, D., Han, L., Borthakur, G., Cortes, J., DeAngelo, D. J., Debose, L., Mu, H., Dohner, H., Gaidzik, V. I., Galinsky, I., Golfman, L. S., Haferlach, T., Harutyunyan, K. G., Hu, J., Levenson, J. D., Marcucci, G., Muschen, M., Newman, R., Park, E., Ruvolo, P. P., Ruvolo, V., Ryan, J., Schindela, S., Zweidler-McKay, P., Stone, R. M., Kantarjian, H., Andreeff, M., Konopleva, M. & Letai, A. G. (2014) Selective BCL-2 inhibition by ABT-199 causes on-target cell death in acute myeloid leukemia, *Cancer Discovery.* **4**, 362-75.

41. Khaw, S. L., Merino, D., Anderson, M. A., Glaser, S. P., Bouillet, P., Roberts, A. W. & Huang, D. C. (2014) Both leukaemic and normal peripheral B lymphoid cells are highly sensitive to the selective pharmacological inhibition of prosurvival Bcl-2 with ABT-199, *Leukemia*. **28**, 1207-15.
42. Karki, S. S., Panjamurthy, K., Kumar, S., Nambiar, M., Ramareddy, S. A., Chiruvella, K. K. & Raghavan, S. C. (2011) Synthesis and biological evaluation of novel 2-aralkyl-5-substituted-6-(4'-fluorophenyl)-imidazo[2,1-b][1,3,4]thiadiazole derivatives as potent anticancer agents, *Eur J Med Chem*. **46**, 2109-16.
43. el-Sherbeny, M. A., el-Bendary, E. R., el-Subbagh, H. I. & el-Kashef, H. A. (1997) Synthesis and cardiotoxic activity of certain imidazo[2,1-b]-1,3,4-thiadiazole derivatives, *Boll Chim Farm*. **136**, 253-6.
44. Pentimalli, L., Milani, G. & Biavati, F. (1975) Preparation and reactivity of imidazo[2,1-b]-1,3,4-thiadiazoles, *Gazzetta Chimica Italiana*. **105**, 777-87.
45. Morris, G. M., Huey, R., Lindstrom, W., Sanner, M. F., Belew, R. K., Goodsell, D. S. & Olson, A. J. (2009) AutoDock4 and AutoDockTools4: Automated docking with selective receptor flexibility, *J Comp Chem*. **30**, 2785-91.
46. Srivastava, M., Hegde, M., Chiruvella, K. K., Koroth, J., Bhattacharya, S., Choudhary, B. & Raghavan, S. C. (2014) Sapodilla plum (*Achras sapota*) induces apoptosis in cancer cell lines and inhibits tumor progression in mice, *Sci Rep*. **4**, 6147.
47. Srivastava, M., Nambiar, M., Sharma, S., Karki, S. S., Goldsmith, G., Hegde, M., Kumar, S., Pandey, M., Singh, R. K., Ray, P., Natarajan, R., Kelkar, M., De, A., Choudhary, B. & Raghavan, S. C. (2012) An inhibitor of nonhomologous end-joining abrogates double-strand break repair and impedes cancer progression, *Cell*. **151**, 1474-87.
48. Moorthy, B. T., Ravi, S., Srivastava, M., Chiruvella, K. K., Hemlal, H., Joy, O. & Raghavan, S. C. (2010) Novel rhodanine derivatives induce growth inhibition followed by apoptosis, *Bioorg Med Chem Let*. **20**, 6297-301.
49. Shahabuddin, M. S., Nambiar, M., Choudhary, B., Advirao, G. M. & Raghavan, S. C. (2010) A novel DNA intercalator, butylamino-pyrimido[4',5':4,5]selenolo(2,3-b)quinoline, induces cell cycle arrest and apoptosis in leukemic cells, *Invest New Drugs*. **28**, 35-48.
50. Vogler, M., Dinsdale, D., Dyer, M. J. & Cohen, G. M. (2013) ABT-199 selectively inhibits BCL2 but not BCL2L1 and efficiently induces apoptosis of chronic lymphocytic leukaemic cells but not platelets, *Brit J Haematol*. **163**, 139-42.
51. Dai, H., Meng, X. W., Lee, S. H., Schneider, P. A. & Kaufmann, S. H. (2009) Context-dependent Bcl-2/Bak interactions regulate lymphoid cell apoptosis, *J Biol Chem*. **284**, 18311-22.
52. Nedelkina, S., Gokce, I., Ridley, H., Weckerle, C., Magnin, T., Vallette, F., Pattus, F., Lakey, J. H. & Bechinger, B. (2008) High-yield expression and purification of soluble forms of the anti-apoptotic Bcl-x(L) and Bcl-2 as TolAIII-fusion proteins, *Protein Expr Purif*. **60**, 214-20.
53. Nambiar, M. & Raghavan, S. C. (2012) Mechanism of fragility at BCL2 gene minor breakpoint cluster region during t(14;18) chromosomal translocation, *J Biol Chem*. **287**, 8688-701.
54. Kavitha, C. V., Choudhary, B., Raghavan, S. C. & Muniyappa, K. (2010) Differential regulation of MRN (Mre11-Rad50-Nbs1) complex subunits and telomerase activity in cancer cells, *Biochem Biophys Res Commun*. **399**, 575-80.
55. Chiruvella, K. K., Kari, V., Choudhary, B., Nambiar, M., Ghanta, R. G. & Raghavan, S. C. (2008) Methyl angolensate, a natural tetranortriterpenoid induces intrinsic apoptotic pathway in leukemic cells, *FEBS Let*. **582**, 4066-76.
56. Kavitha, C. V., Nambiar, M., Ananda Kumar, C. S., Choudhary, B., Muniyappa, K., Rangappa, K. S. & Raghavan, S. C. (2009) Novel derivatives of spirohydantoin induce growth inhibition followed by apoptosis in leukemia cells, *Biochem Pharmacol*. **77**, 348-63.
57. Kavitha, C. V., Nambiar, M., Narayanaswamy, P. B., Thomas, E., Rathore, U., Ananda Kumar, C. S., Choudhary, B., Rangappa, K. S. & Raghavan, S. C. (2013) Propyl-2-(8-(3,4-difluorobenzyl)-2',5'-dioxo-8-azaspiro[bicyclo[3.2.1] octane-3,4'-imidazolidine]-1'-yl) acetate induces apoptosis in human leukemia cells through mitochondrial pathway following cell cycle arrest, *PLoS One*. **8**, e69103.

Table 1. Table showing the chemical and physical characterisation of reaction intermediates during the synthesis of potential BCL2 inhibitors. Compound series **3a-3o** and **4a-4o, 4s, 4t** are the intermediates formed during the synthesis of compounds described in Figure 1C. Compound characteristics such as alkyl group substitutions, molecular weight (Mol Wt), molecular formula (Mol For) and melting points (MP) are listed.

Structure	Code No	R	R'	Mol Wt	Mol For	MP (°C)
 3a-3o	3a	benzyl	4-Br-phenyl	370.27	C ₁₇ H ₁₂ BrN ₃ S	170-172
	3b	benzyl	4-Cl-phenyl	325.82	C ₁₇ H ₁₂ ClN ₃ S	163-165
	3c	benzyl	4-OCH ₃ -phenyl	321.40	C ₁₈ H ₁₅ N ₃ OS	180-182
	3d	benzyl	4-CH ₃ -phenyl	305.40	C ₁₈ H ₁₅ N ₃ OS	160-162
	3e	4-Cl-benzyl	phenyl	325.82	C ₁₇ H ₁₂ ClN ₃ S	193-195
	3f	4-Cl-benzyl	4-Cl-phenyl	360.27	C ₁₇ H ₁₁ Cl ₂ N ₃ S	178-179
	3g	4-Cl-benzyl	4-CH ₃ -phenyl	339.85	C ₁₈ H ₁₄ ClN ₃ S	178-181
	3h	4-Cl-benzyl	4-OCH ₃ -phenyl	355.85	C ₁₈ H ₁₄ ClN ₃ OS	174-176
	3i	benzyl	4-F-phenyl	309.37	C ₁₇ H ₁₂ FN ₃ S	152-155
	3j	benzyl	phenyl	291.38	C ₁₇ H ₁₃ N ₃ S	163-165
	3k	benzyl	4-NO ₂ -phenyl	336.37	C ₁₇ H ₁₂ N ₄ O ₂ S	219-222
	3l	4-Cl-benzyl	4-NO ₂ -phenyl	370.82	C ₁₇ H ₁₁ ClN ₄ O ₂ S	195-198
	3m	4-Cl-benzyl	4-Br-phenyl	404.72	C ₁₇ H ₁₁ BrClN ₃ S	164-165
	3n	4-Cl-benzyl	4-F-phenyl	343.81	C ₁₇ H ₁₁ FCIN ₃ S	167-170
	3o	4-Cl-benzyl	2 <i>H</i> -chromen-2-one	393.85	C ₂₀ H ₁₂ ClN ₃ O ₂ S	202-205
 4a-4o, 4s, 4t	4a	benzyl	4-Br-phenyl	398.28	C ₁₈ H ₁₂ BrN ₃ OS	126-128
	4b	benzyl	4-Cl-phenyl	353.83	C ₁₈ H ₁₂ ClN ₃ OS	183-185
	4c	benzyl	4-OCH ₃ -phenyl	349.41	C ₁₉ H ₁₅ N ₃ O ₂ S	160-162
	4d	benzyl	4-CH ₃ -phenyl	333.41	C ₁₉ H ₁₅ N ₃ OS	107-108
	4e	4-Cl-benzyl	phenyl	353.83	C ₁₈ H ₁₂ ClN ₃ OS	119-121
	4f	4-Cl-benzyl	4-Cl-phenyl	388.28	C ₁₈ H ₁₁ Cl ₂ N ₃ OS	118-120
	4g	4-Cl-benzyl	4-CH ₃ -phenyl	367.86	C ₁₉ H ₁₄ ClN ₃ OS	83-85
	4h	4-Cl-benzyl	4-OCH ₃ -phenyl	383.86	C ₁₉ H ₁₄ ClN ₃ O ₂ S	101-104
	4i	benzyl	4-F-phenyl	337.38	C ₁₈ H ₁₂ FN ₃ OS	112-114
	4j	benzyl	phenyl	319.39	C ₁₈ H ₁₃ N ₃ OS	145-147
	4k	benzyl	4-NO ₂ -phenyl	364.39	C ₁₈ H ₁₂ N ₄ O ₃ S	136-138
	4l	4-Cl-benzyl	4-NO ₂ -phenyl	398.83	C ₁₈ H ₁₁ ClN ₄ O ₃ S	157-159
	4m	4-Cl-benzyl	4-Br-phenyl	432.73	C ₁₈ H ₁₁ ClBrN ₃ O S	129-131
	4n	4-Cl-benzyl	4-F-phenyl	371.82	C ₁₈ H ₁₁ ClFN ₃ OS	138-140
	4o	4-Cl-benzyl	2 <i>H</i> -chromen-2-one	421.87	C ₂₁ H ₁₂ ClN ₃ O ₃ S	130-133
4s	CH ₃	4-CH ₃ -phenyl	257.31	C ₁₃ H ₁₁ N ₃ OS	130-132	
4t	CH ₃	4-OCH ₃ -phenyl	273.31	C ₁₃ H ₁₁ N ₃ O ₂ S	50-52	

* decomposed

Table 2. Table showing comparison of IC₅₀ values of the synthesized small molecules, based on their cytotoxicity in NALM6, K562 and CEM cell lines. IC₅₀ values were based on cell proliferation as assayed by MTT at 48 h following addition of compounds. Percentage of cell proliferation was plotted relative to cells treated with DMSO, the vehicle control. In each case, experiments were performed a minimum of three times, data is presented as mean ± SEM.

Compound	NALM6	K562	CEM
5a	3.0	3.25	11.0
5b	14.0	2.75	6.0
5c	25	4.75	26.0
5e	25.0	13.5	2.5
5f	20.5	3.25	17.0
5g	2.5	2.75	23.25
5i	12.5	5.0	42.5
5j	25.0	17.5	5.0
5l	62.5	12.5	15.0
5m	2.53	31.00	2.46
5n	10.0	15.0	47.5
5o	2.0	3.5	20.25
5p	41.87	40	50
5q	50.37	15.62	28.12
5r	>125	45	50
5s	35.0	37.5	39.37
5t	10.0	70.0	13.75

Table 3. Table summarizing the interactions between Disarib and BH1 domain of various antiapoptotic proteins. Amino acid residue number is with reference to BCL2. Plus (+) and minus (-) indicate the presence and absence of interactions, respectively. Note the emergence of 2 additional strong interactions in MCL1 when its BH1 domain is swapped with that of BCL2 (gray coloured box). Amino acid residue corresponding to BCL2 R139, in wild type MCL1 (V) and BCL-W (L) that displayed interaction with Disarib is enclosed in bracket for reference.

Antiapoptotic protein	Interaction of Disarib with amino acid residues of BH1 domain of different antiapoptotic proteins.				
	N 143 (Highly conserved)	W 144 (Highly conserved)	G 145 (Highly conserved)	R146 (Highly conserved)	R 139 (partially conserved)
BCL2	+	+	+	+	+
MCL1 (<i>wild</i>)	+	-	+	-	+(V)
BCL-xL	+	-	+	-	-
BCL2A1	-	-	+	+	-
BCLW	+	-	-	+	+(L)
MCL1 with <i>BH1</i> <i>Domain swapped</i> <i>from BCL2</i>	+	-	+	+	+

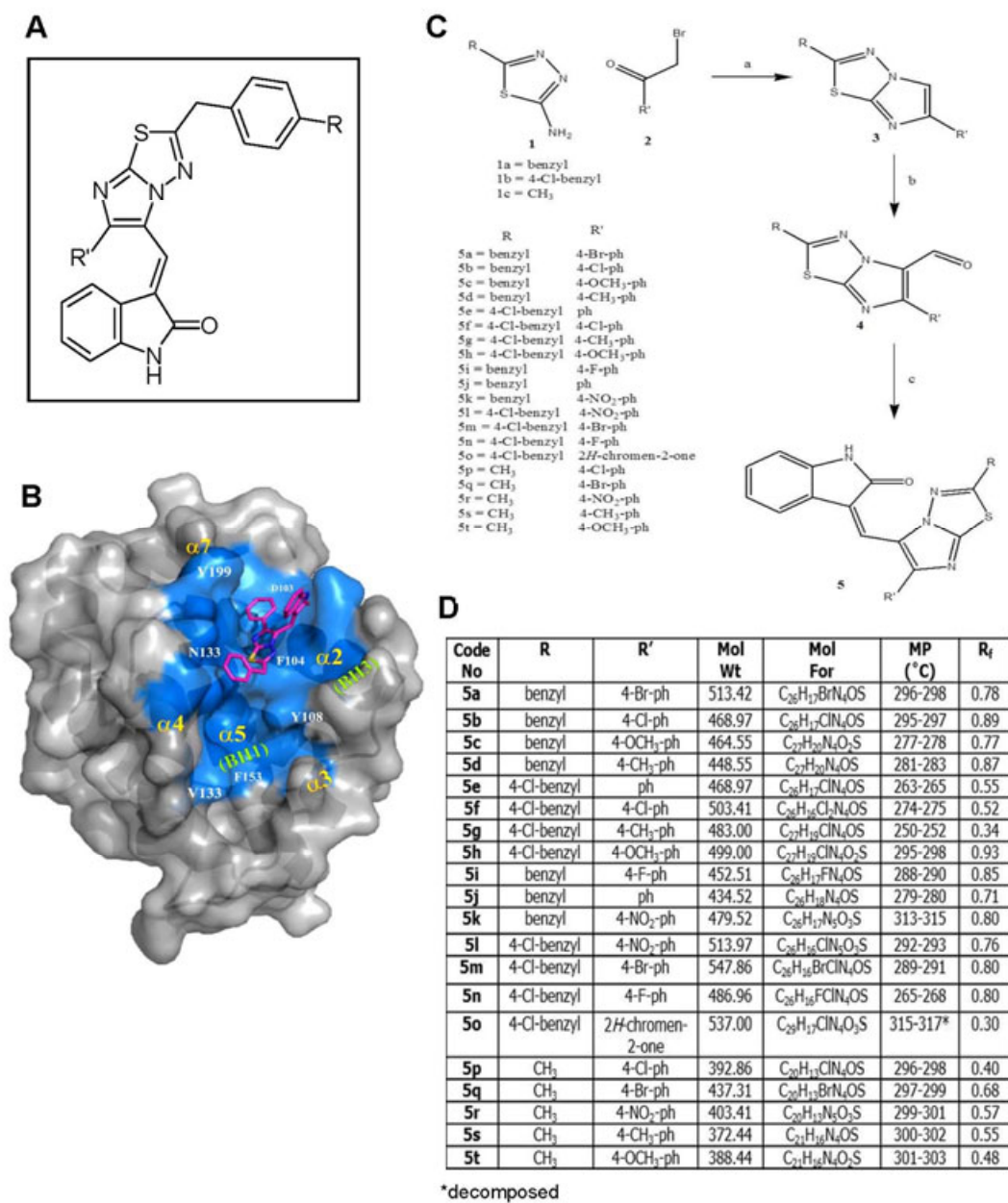


Figure 1

Figure 1. Design, synthesis, biochemical and biological characterization of potential BCL2 inhibitors. **A.** Basic chemical backbone of compound series **5**, used for evaluating BCL2 affinity. **B.** Docked orientation of compound **5** (pink sticks) in the putative binding pocket (blue) along the hydrophobic groove of BCL2 (gray surface). Residues (white) forming the putative binding pocket and domains BH1 and BH3 of BCL2 are indicated. **C.** Scheme for chemical synthesis of the molecular backbone of potential BCL2 inhibitors, **5a-5t**. Alcohol, sodium carbonate (a), POCl₃, DMF, 80-90°C (b), 2-indoliaone, CH₃OH, piperidine, 30 min (c). **D.** Table summarising the chemical characterisation of the panel of synthesized compounds, which includes compound code, nature of the side chain alkyl groups (R, R'), molecular weight (Mol Wt), molecular formula (Mol Formula), melting points (MP), and R_f (retardation factor). “*” indicates decomposed stage.

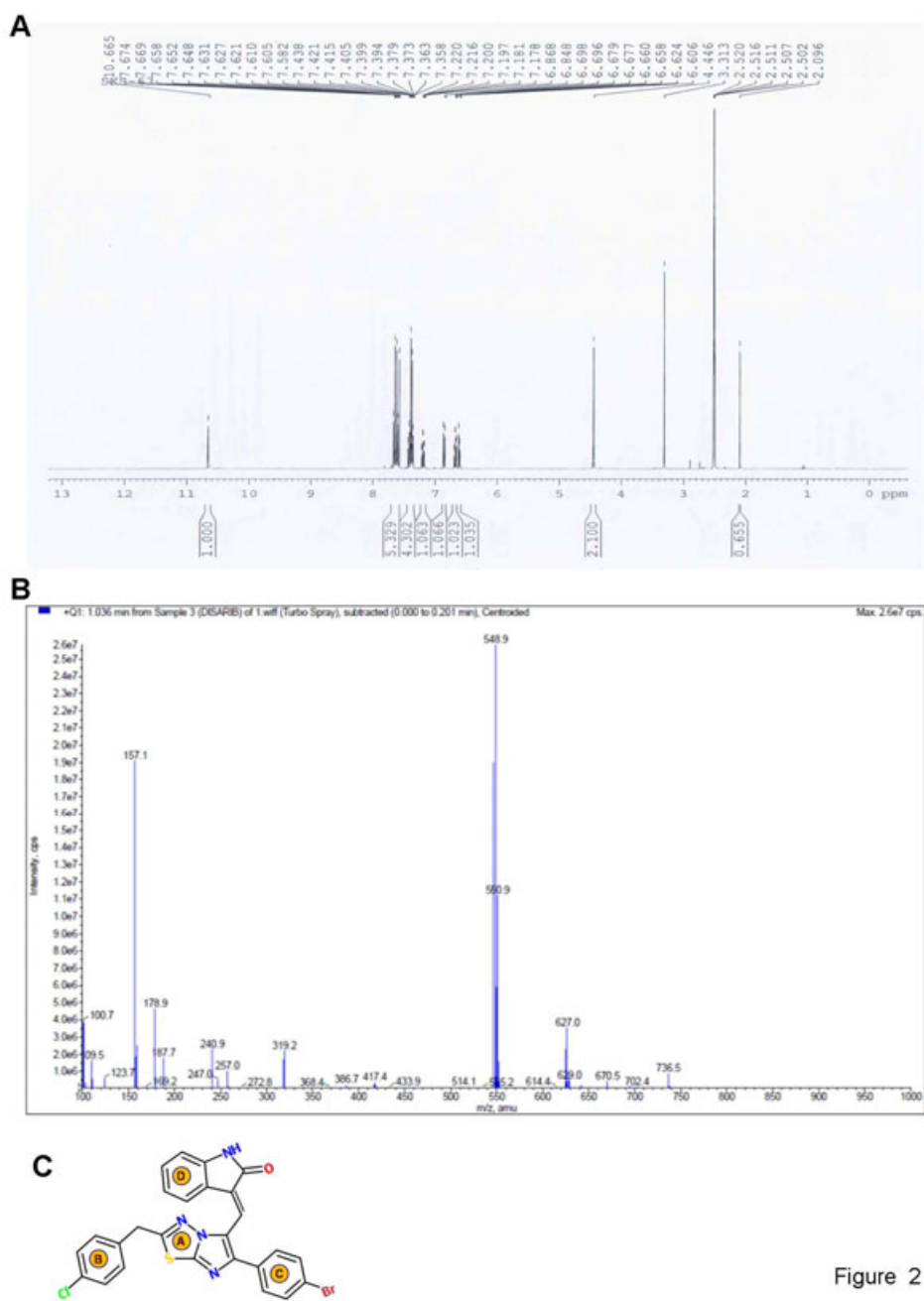


Figure 2

Figure 2. Biophysical characterization of Disarib. **A.** NMR spectrum of Disarib, used for elucidating the chemical structure. **B.** LC-MS spectrum of Disarib for evaluating the purity of compound. **C.** Chemical structure of **5m** (Disarib).

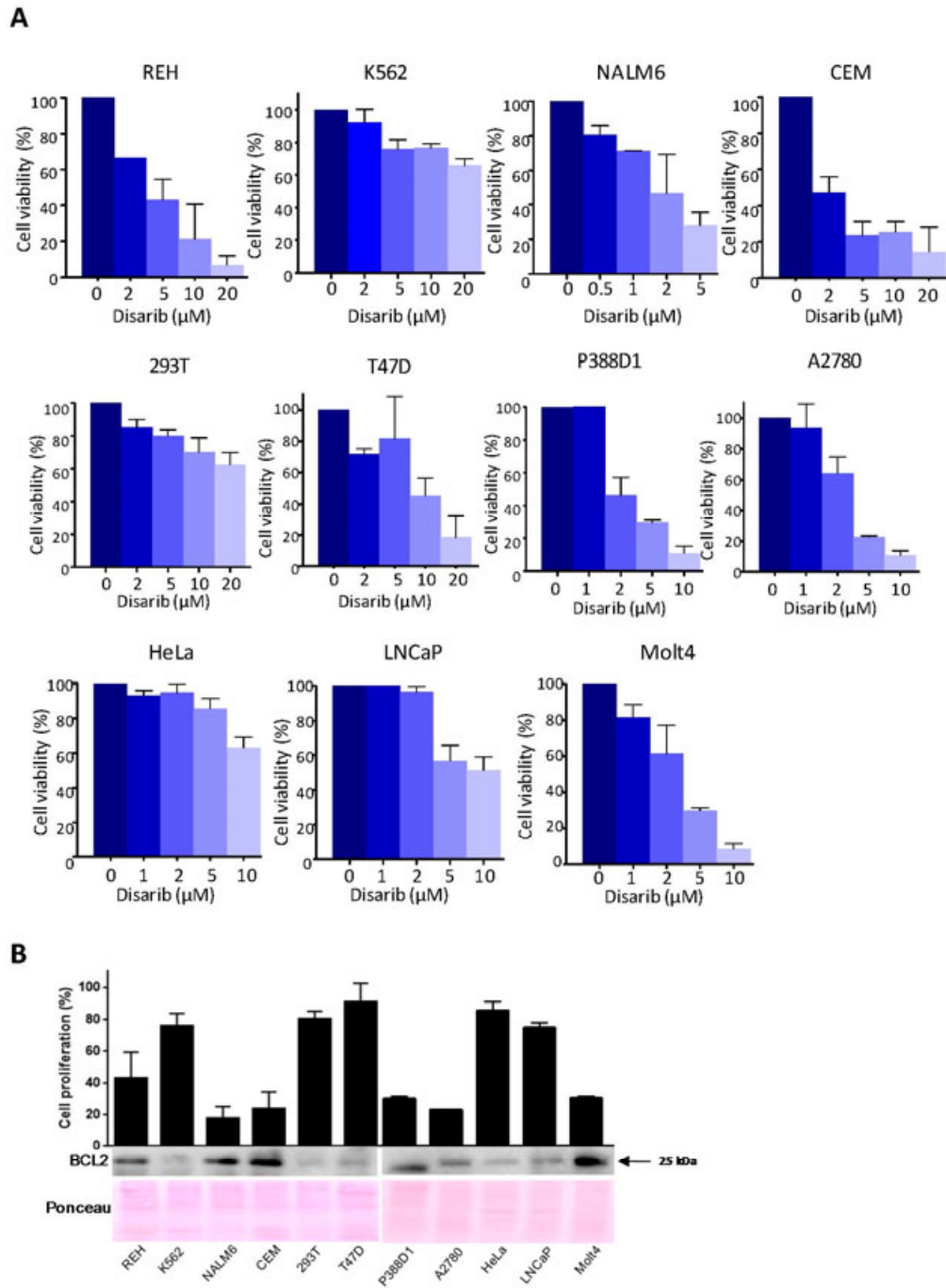


Figure 3. Evaluation of cytotoxicity induced by Disarib in various cancer cell lines and its correlation with BCL2 expression. **A.** Evaluation of cytotoxicity following treatment with Disarib (for 48 h) in various cell lines. In case of REH, K562, HEK 293T, CEM and T47D cells, concentration of 2, 5, 10 and 20 μM of Disarib was used, while in P388D1, A2780, HeLa, LNCaP and Molt4, 1, 2, 5 and 10 μM was administered and cell death was assayed by trypan blue dye exclusion assay. In case of NALM6, concentration of Disarib used were 0.5, 1, 2 and 5 μM as it was more sensitive compared to other cell lines. Experiments were performed a minimum of three times and graph shows mean \pm SEM. **B.** Evaluation of cytotoxicity following treatment with Disarib in various cell lines described in panel A and analysis of endogenous BCL2 expression. Cell viability was determined after 48 h of Disarib (5 μM) treatment. The graph shows mean \pm SEM (n = 3). Lower panel shows endogenous levels of BCL2 as determined by western blotting in various cell lines. Experiments were repeated a minimum of three times and representative blot is presented. Ponceau stained blot was used as a loading control.

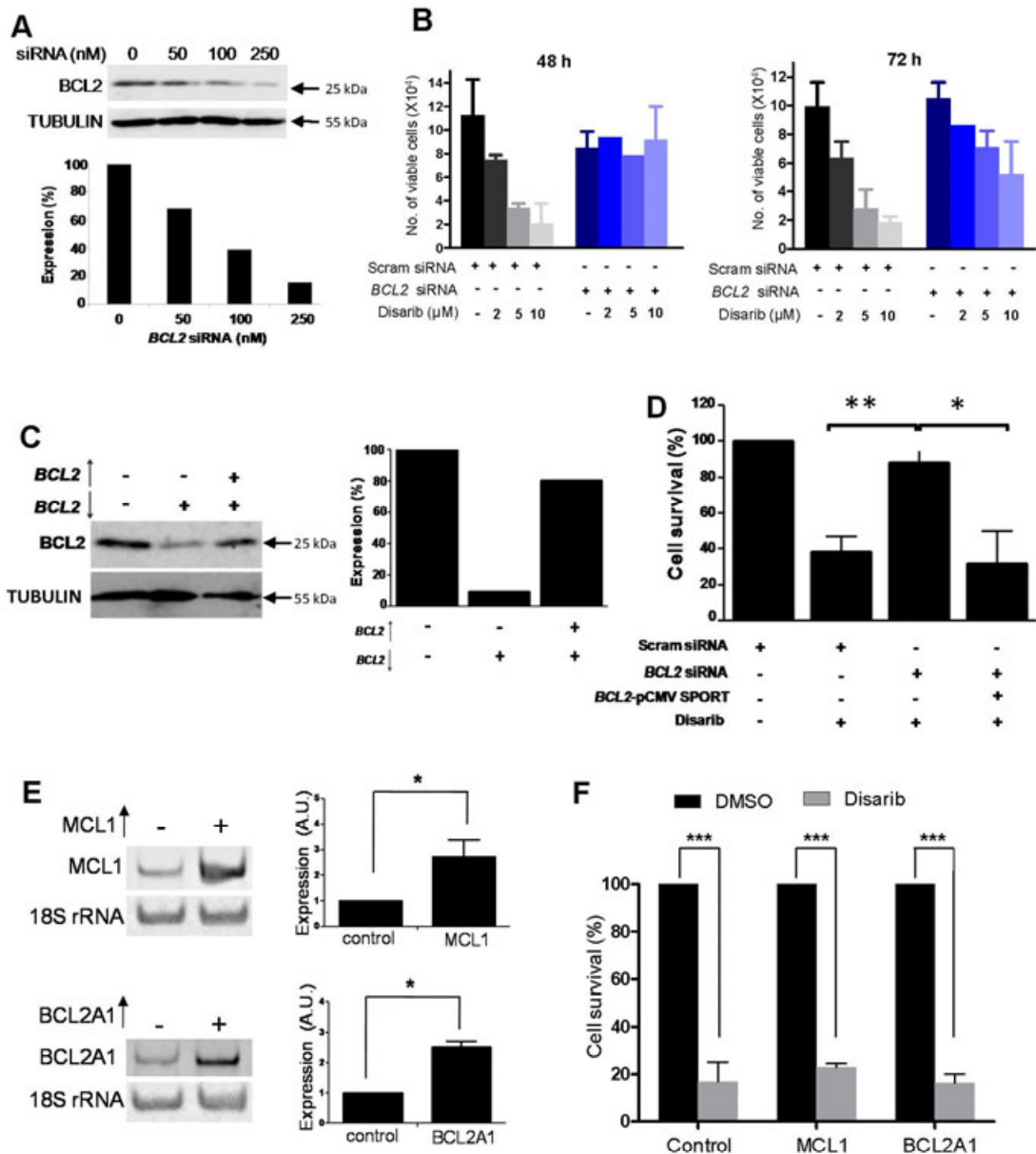


Figure 4

Figure 4. Knockdown and overexpression studies for BCL2 specific action of Disarib. **A.** Western blot showing BCL2 levels in NALM6 cells following transfection with *BCL2* siRNA (0, 50, 100 and 250 nM). The level of BCL2 knockdown is quantified and presented. **B.** Bar diagram showing comparison of Disarib induced cytotoxicity (48, 72 h) in NALM6 cells following knockdown of BCL2. Cells were transfected with scrambled siRNA (250 nM) or *BCL2* siRNA (250 nM), 24 h prior to treatment with Disarib (0, 2, 5 and 10 μ M). Experiments were repeated (n = 3) and the graph was plotted as \pm SEM. **C.** Western blot showing BCL2 levels in NALM6 cells treated with vehicle control, *BCL2* siRNA or *BCL2* siRNA followed by *BCL2* overexpression vector. Quantification showing the levels of BCL2 expression in terms of relative photostimulated luminescence (PSL) units is presented in the right panel. Expression level of BCL2 in the vehicle control is designated as 100%. **D.** Bar diagram showing the effect of Disarib (5 μ M, 48 h), on the viability of NALM6 cells containing endogenous, knocked down and restored levels of BCL2. In all cases, percentage of cell viability is relative to NALM6 cells treated with appropriate vehicle controls for the same period. In panel d, graph shows mean \pm SEM (ns: not significant, *p < 0.05, **p < 0.005, ***p < 0.0001). In each case, experiments were repeated (n = 3). **E.** Overexpression profiles of MCL1 and BCL2A1 in NALM6 cells, as tested by RT PCR. 18S rRNA was used as a loading control for cDNA in both the cases. Each experiment was repeated (n = 2), and a quantification of relative band intensities of both the genes is presented as a bar graph showing mean \pm SEM (right panel). **F.** Bar diagram depicting the effect of Disarib (5 μ M, 48 h) on cells overexpressing MCL1 and BCL2A1, in addition to transfected control group. In each case, percentage of cell survival is expressed relative to that in vehicle control cells.

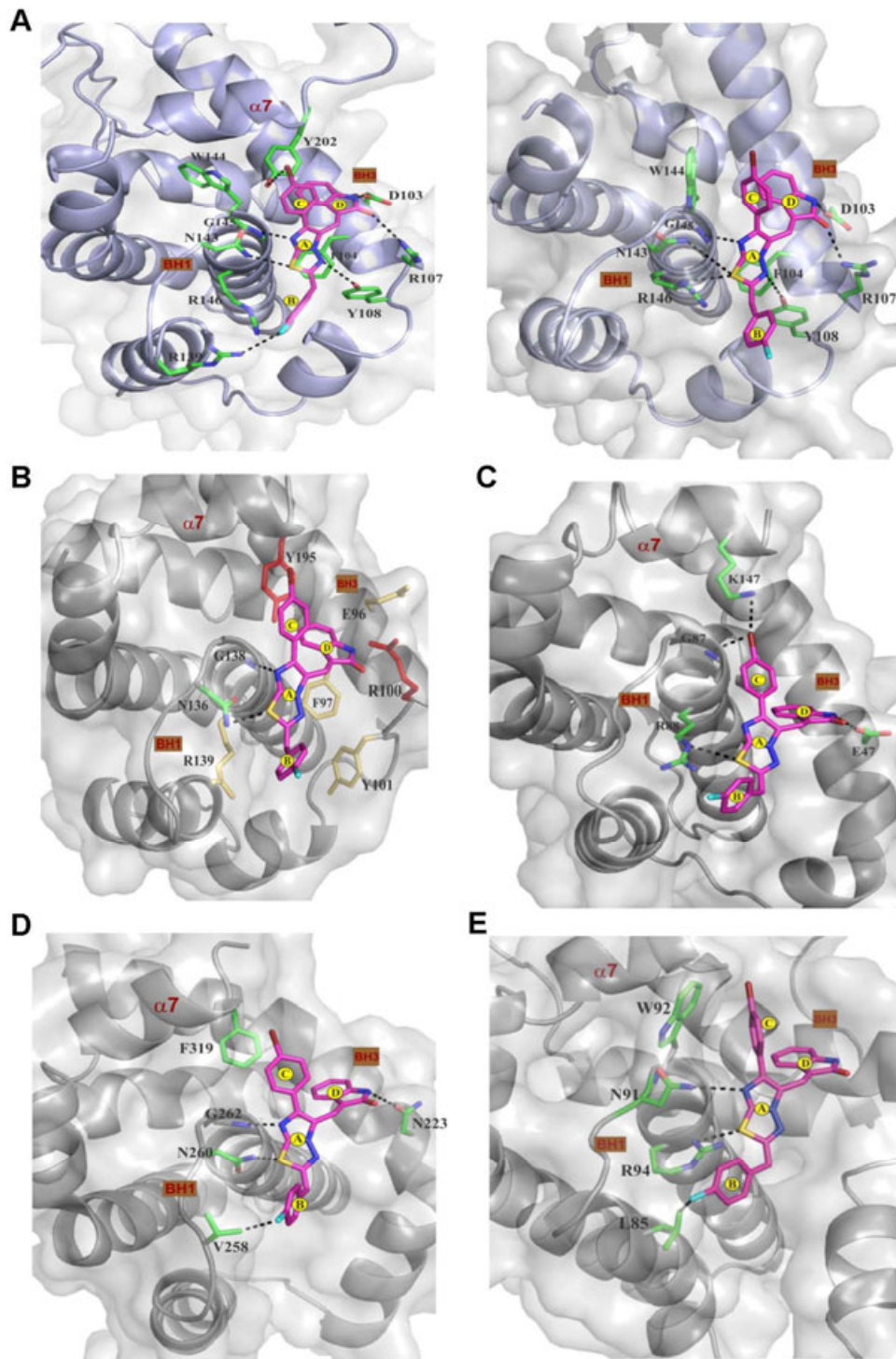


Figure 5

Figure 5. *In silico* analyses of Disarib binding to various antiapoptotic family proteins. A. Interaction between Disarib (pink sticks) and amino acid residues (green sticks) along the putative binding pocket of BCL2 (both full length and Δt_m domain) (light blue; PDB ID: 1GJH). Hydrogen bond interactions are depicted as dashes. **B.** Docked complex of Disarib and BCL-xL (PDB ID: 1R2D). Note the comparatively less number of stabilizing interactions between Disarib and BCL-xL (gray cartoon), than Disarib and BCL2 shown in the panel A. Observed reduced binding affinity may be due to short contacts involving Disarib and R100 and Y195 (red sticks). Equivalent residues that exhibited interaction with Disarib in BCL2 but not in BCL-xL are shown as gold coloured sticks. **C-E.** Interaction of Disarib with other antiapoptotic proteins viz., BCL2A1 (C), MCL1 (D) and BCL-w (E). Residues exhibiting interaction with Disarib are depicted as green sticks. BH1, BH3 domains and helix $\alpha 7$ are indicated.

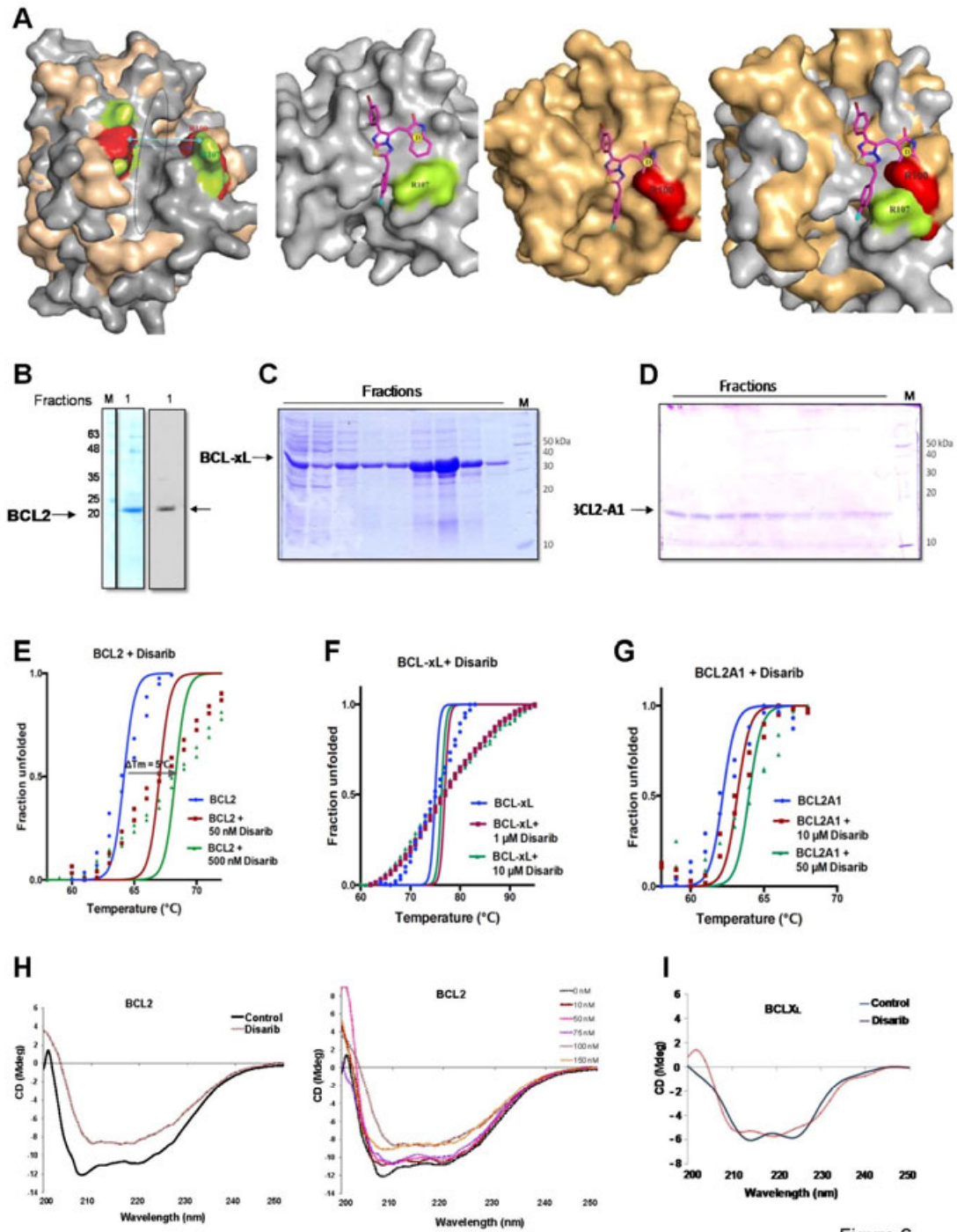


Figure 6

Figure 6. Analyses of interaction of Disarib with BCL2 and other antiapoptotic proteins BCL-xL and BCL2A1. **A.** Top figure shows superposition of BCL2 (gray) and BCL-xL (light brown) surface diagrams to indicate the difference in putative binding pocket width along the hydrophobic groove (black ellipse). Widths are indicated by cyan and blue arrows for BCL2 and BCL-xL, respectively. Comparison of docked complex of Disarib (pink sticks) with BCL2 (gray surface) and with BCL-xL (brown surface) (middle panel). In case of BCL2, conserved Arg 107 adjoining the binding groove is marked. Presence of ring D leads to short contacts with R100 in BCL-xL, whereas it is not so in case of BCL-2 due to differential spatial presence of Arginine residue in BCL2 vs BCL-xL which is shown as lower panel. **B-D.** Overexpression and purification of various BCL2 family proteins. SDS-PAGE profiles showing eluted fractions of purified proteins, BCL2 (B), BCL-xL (C), BCL2A1 (D). In each case, fractions were loaded onto SDS-PAGE, and visualized using CBB staining. In all cases, the protein band of interest is denoted by an arrow. 'M' indicates marker. In panel C, immunoblot confirmation of BCL2 is also shown. **E-G.** Effect of Disarib on the thermal melting of BCL2 family proteins. A thermal shift of about 5°C was observed in case of BCL2 with 50 nM to 500 nM Disarib (E). Only marginal shift in thermal melting was observed for other homologs, BCL-xL (F) and BCL2A1 (G) at high Disarib concentrations. **H.** CD spectra showing changes in the secondary structure of BCL2 (9 μM) upon incubation with 100 nM (left panel) or different concentrations of Disarib (0, 10, 50, 75,100,150 nM) (right panel). The spectra were recorded in the far-UV range between 200-250 nm. **I.** CD spectrum showing changes in the secondary structure of BCL-xL (6 μM) upon incubation with Disarib (0.5 μM).

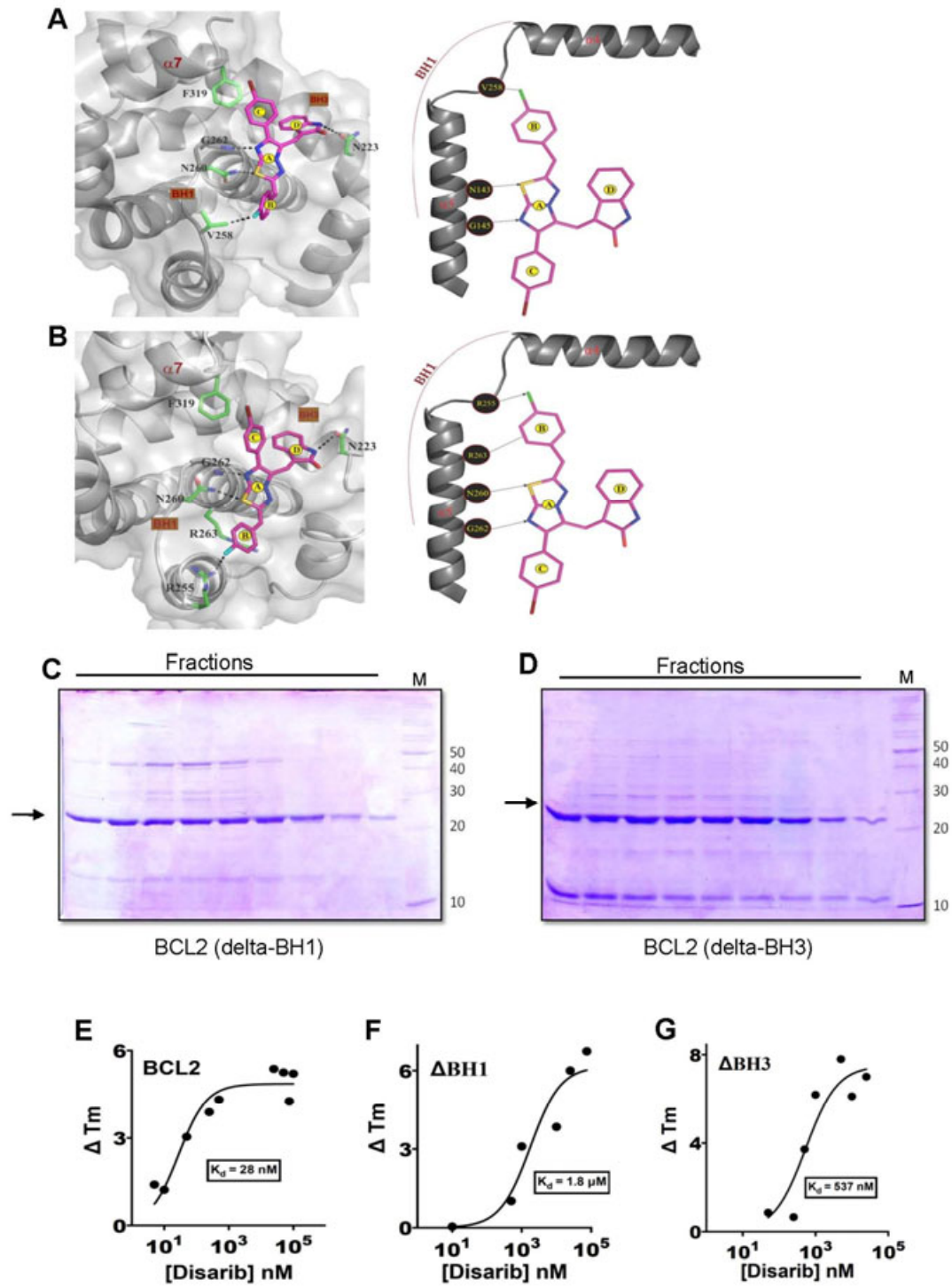


Figure 7. Evaluation of preferential binding of Disarib to the BH1 domain of BCL2. **A,B.** Docked complex of Disarib (pink sticks) with wild type (A) and domain swapped (B) MCL1 structures. Schematic representation of the interaction involving only the BH1 domain and Disarib in their respective states is shown in right panel. Hydrogen bond interaction is depicted as dashed line with arrow head, while cation- π /van der Waals interaction is shown as dashed line. Note the increase in number of interactions (3 \rightarrow 4) arising between BH1 domain of MCL1 in domain swapped state and Disarib. Interactions emanating from the BH3 domain and helix α 7 remain common (N223 and F319) in both wild and domain swapped structures. Residues exhibiting interaction with Disarib are depicted as green sticks. BH1, BH3 domains and helix α 7 are labelled. **C,D.** SDS-PAGE profiles showing eluted fractions of purified proteins, BCL2 with BH1 domain deleted (C) and BCL2 with BH3 domain deleted (D). **E.** Net change in T_m of BCL2 protein with increasing concentration of Disarib, as determined by the thermal shift assay. **F,G.** Net change in T_m of two domain deletion constructs of BCL2: Δ BH1 (F) and Δ BH3 (G) against increasing concentration of Disarib.

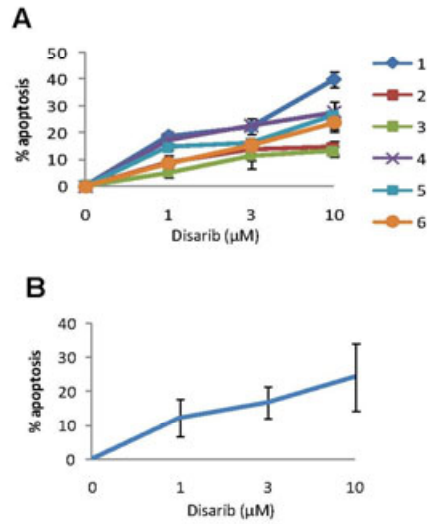


Figure 8

Figure 8. Evaluation of Disarib-induced cytotoxicity in CLL patient primary cells. A. Cells from six (CLL) patients were incubated in presence of the indicated concentrations of Disarib for 4 h. Level of apoptosis was determined using Annexin V-FITC binding and FACS. Data is presented as % apoptosis observed above the level of spontaneous apoptosis. **B.** The average % apoptosis from different patients (n = 6) is plotted as a graph showing mean \pm SEM.

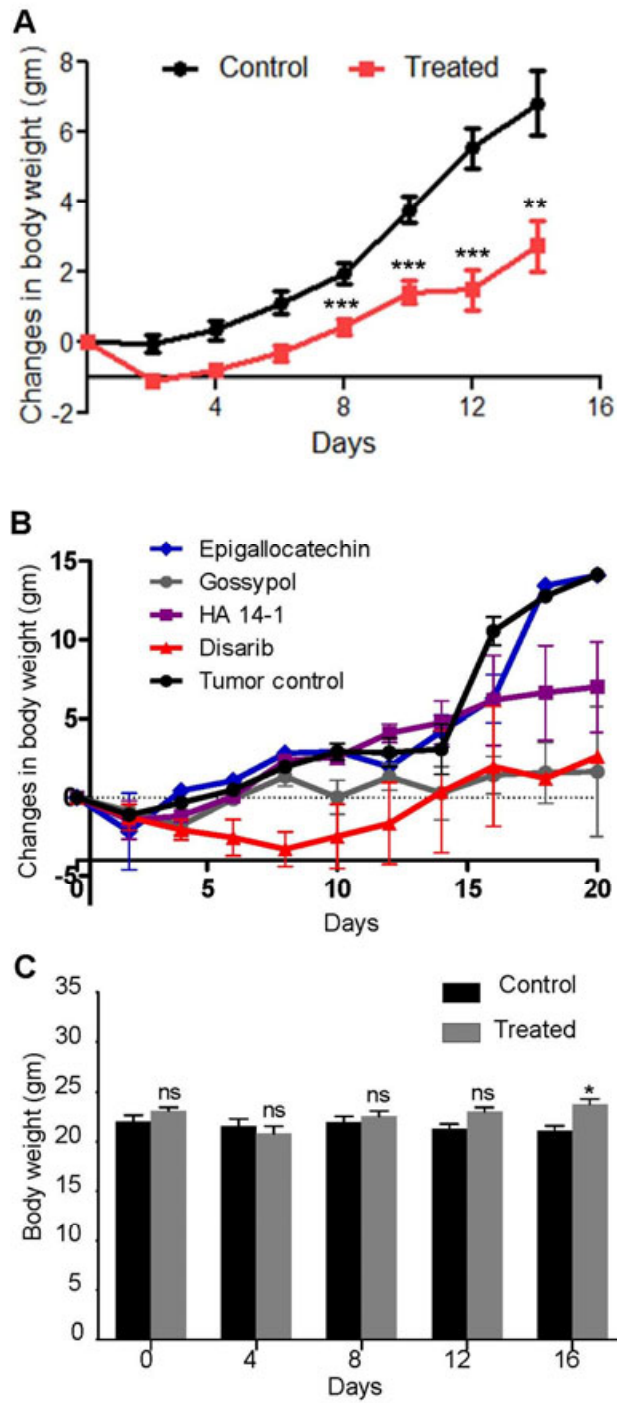


Figure 9

Figure 9. Evaluation of effect of Disarib on tumor cell proliferation in a BCL2-driven mouse tumor model. **A.** Graph showing the effect of Disarib on tumor cell proliferation in mouse. Tumor was generated using Dalton's lymphoma (DLA) cells and was treated with Disarib (10 mg/kg, 6 doses, alternate day, n=6, 4 batches). Tumor progression was monitored by measuring the changes in body weight, normalized to the weight fluctuations in normal mice. **B.** Graph showing comparative analysis of tumor growth inhibition properties of known BCL2 inhibitors, HA 14-1, Gossypol and Epigallocatechin, along with Disarib (10 mg/kg, 6 doses, alternate day, n=5, 2 batches). **C.** Bar graph showing body weight measurements of Disarib treated normal mice (gray bars) in comparison with those in untreated control group (black bars) (n = 10 in each case). The graph shows mean \pm SEM (ns: not significant, *p < 0.05, **p < 0.005, ***p < 0.0001).

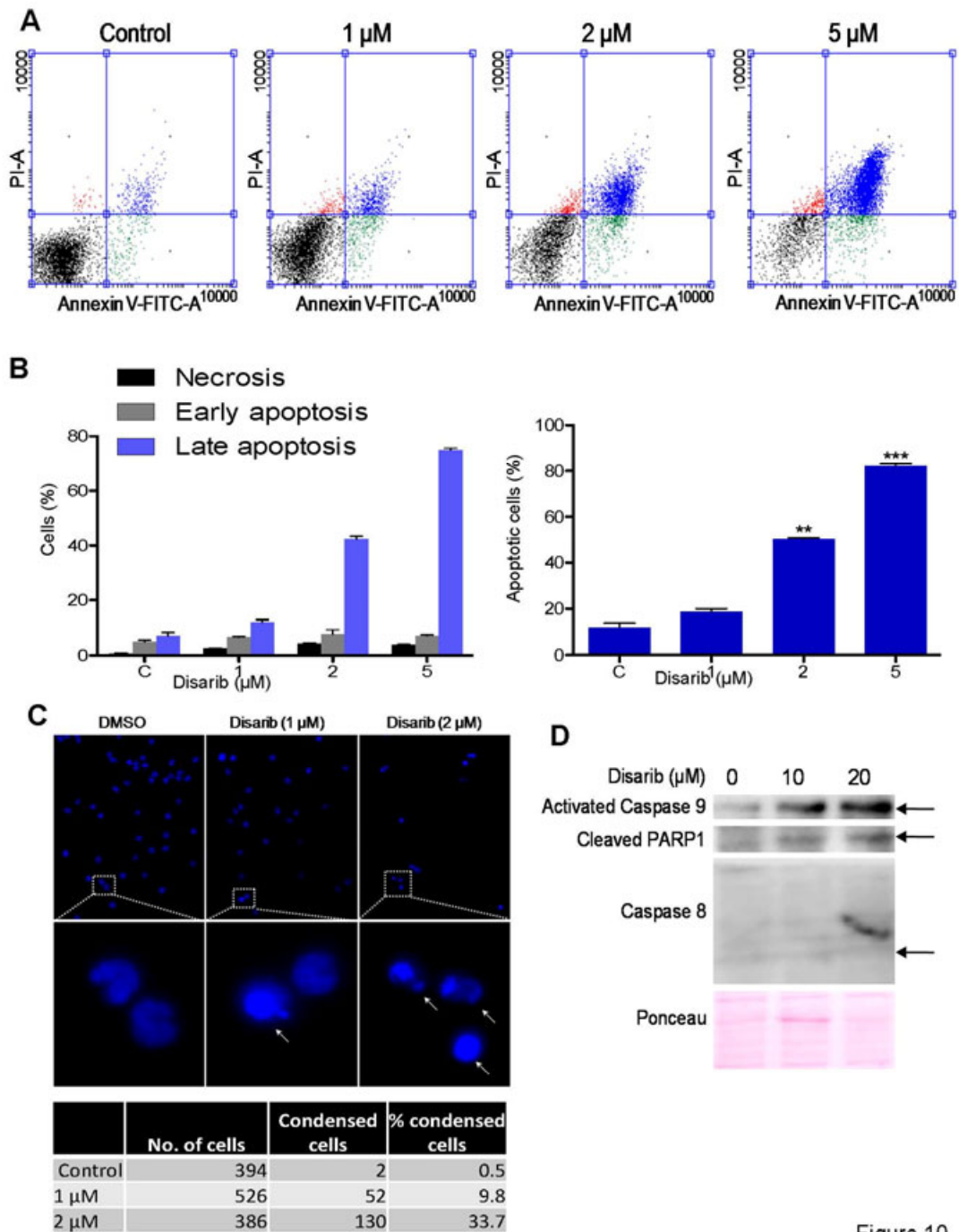


Figure 10

Figure 10. Investigation of the mode of Disarib-induced cell death. **A.** Annexin V-FITC and PI double-staining for evaluation of the mode of cytotoxicity induced by Disarib. Molt4 cells treated with Disarib (1, 2 and 5 μ M, 48 h), stained with Annexin V-FITC and PI, and subjected to flow cytometry analyses. Lower left quadrant shows cells negative for Annexin V-FITC/ PI staining, the lower right quadrant for only Annexin V-FITC staining (early apoptotic cells), upper left quadrant for PI positive cells (necrosis) and upper right quadrant for both Annexin V-FITC and PI positive cells (late apoptosis). **B.** Bar graphs depicting quantification of necrotic, early apoptotic and late apoptotic cell populations (left panel) and combined quantification of apoptotic cells (right panel). Each experiment was repeated (n= 3), and the bar graphs plotted mean \pm SEM. (ns: not significant, *p < 0.05, **p < 0.005, ***p < 0.0001). **C.** Representative microscopic images depicting Hoechst stained Molt4 cells, following Disarib treatment, along with an untreated control (10X). Individual nuclear morphology is boxed and enlarged for each concentration and presented in the lower panel. Arrows depict condensed and fragmented nuclei. Quantification of number of Molt4 cells showing nuclear condensation post Disarib treatment (1 and 2 μ M, 48 h), as compared to an untreated control is presented as a table in the lower panel. **D.** Panel showing western blot analysis for apoptotic markers Caspase 9, PARP and Caspase 8, for DLA tumor cells treated with increasing concentrations of Disarib (0, 10, 20 μ M). Unlike above panels, the Disarib concentrations used were higher as the cells used were from mouse tumor ascitic fluid. Ponceau stained blot served as loading control. The expected molecular weight position of each protein is indicated by an arrow. Each experiment was repeated (n = 3), and a representative blot is presented.

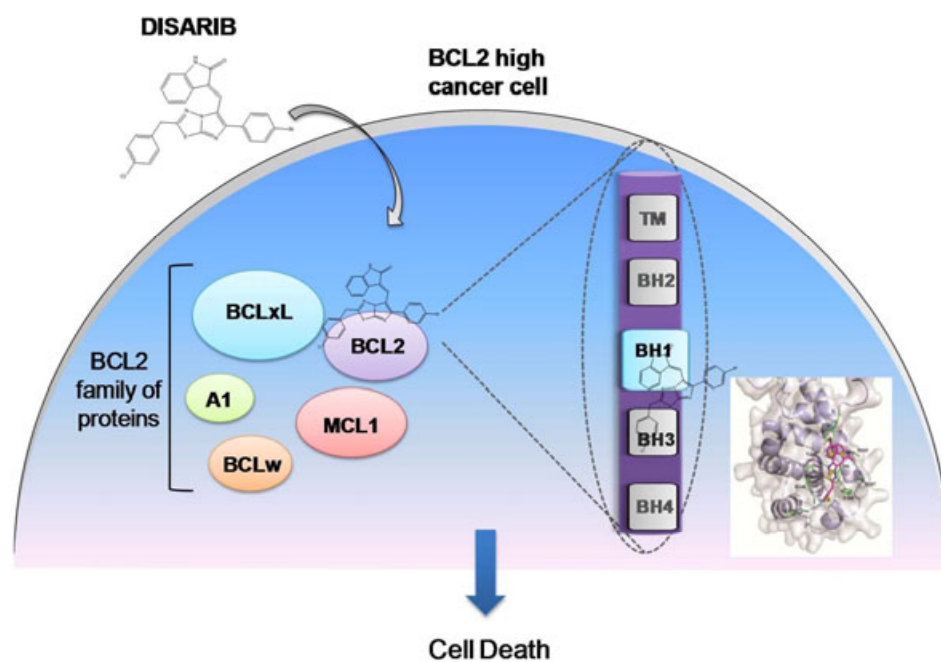


Figure 11

Figure 11. Model illustrating the putative mechanism of action of Disarib in cancer cells. Disarib acts on BCL2 high cancer cells by specifically binding to and inhibiting BCL2 function, while sparing other anti-apoptotic proteins such as BCL-xL, MCL1, BCLw and BCL2A1. It predominantly targets the BH1 domain of BCL2, thus exhibiting a novel mode of BCL2 inhibition, ultimately leading to cell death.